

Kaon B parameter from quenched domain-wall QCD

A. Ali Khan,¹ S. Aoki,² Y. Aoki,^{1,2,*} R. Burkhalter,^{1,2} S. Ejiri,^{1,†} M. Fukugita,³ S. Hashimoto,⁴ N. Ishizuka,^{1,2} Y. Iwasaki,^{1,2}
T. Izubuchi,^{5,‡} K. Kanaya,² T. Kaneko,⁴ Y. Kuramashi,⁴ K. I. Nagai,^{1,§} M. Okawa,⁴ H. P. Shanahan^{1,||} Y. Taniguchi,²
A. Ukawa,^{1,2} and T. Yoshie^{1,2}

(CP-PACS Collaboration)

¹*Center for Computational Physics, University of Tsukuba, Tsukuba, Ibaraki 305-8577, Japan*

²*Institute of Physics, University of Tsukuba, Tsukuba, Ibaraki 305-8571, Japan*

³*Institute for Cosmic Ray Research, University of Tokyo, Kashiwa 277-8582, Japan*

⁴*High Energy Accelerator Research Organization (KEK), Tsukuba, Ibaraki 305-0801, Japan*

⁵*Institute of Theoretical Physics, Kanazawa University, Ishikawa 920-1192, Japan*

(Received 21 May 2001; published 8 November 2001)

We report on a calculation of B_K with domain-wall fermion action in quenched QCD. Simulations are made with a renormalization group improved gauge action at $\beta=2.6$ and 2.9 corresponding to $a^{-1}\approx 2$ and 3 GeV. Effects due to finite fifth dimensional size N_5 and finite spatial size N_σ are examined in detail. Matching to the continuum operator is made perturbatively at one loop order. We obtain $B_K(\mu=2 \text{ GeV})=0.5746(61)(191)$, where the first error is statistical and the second error represents an estimate of scaling violation and $\mathcal{O}(\alpha^2)$ errors in the renormalization factor added in quadrature, as an estimate of the continuum value in the modified minimal subtraction (MS) scheme with naive dimensional regularization. This value is consistent, albeit somewhat small, with $B_K(\mu=2 \text{ GeV})=0.628(42)$ obtained by the JLQCD Collaboration using the Kogut-Susskind quark action. Results for light quark masses are also reported.

DOI: 10.1103/PhysRevD.64.114506

PACS number(s): 11.15.Ha, 12.38.Gc

I. INTRODUCTION

The kaon B parameter B_K is an important quantity to pin down the Cabibbo-Kobayashi-Maskawa matrix from experiment, thereby advancing our understanding of CP violation in the standard model [1].

A crucial ingredient in a precision calculation of B_K is chiral symmetry. Without this symmetry the relevant $\Delta S = 2$ four-quark operator mixes with other operators of different chiralities. It is a nontrivial task to accurately determine the mixing coefficients.

This problem has caused significant difficulties with calculations using the Wilson-type fermion action, which has explicit chiral symmetry breaking. While several non-perturbative methods have been developed to determine the mixing coefficients [2–4], the numerical errors in the values of B_K obtained with these methods are still quite large [1].

The situation is better with the Kogut-Susskind fermion action for which $U(1)$ subgroup of chiral symmetry, valid at finite lattice spacings, ensures the correct chiral behavior of the matrix element [5]. Exploiting this feature a systematic

and extensive set of simulations have been carried out [6]. Taking into account $\mathcal{O}(a^2)$ scaling violation and $\mathcal{O}(\alpha_{\overline{\text{MS}}}^2)$ errors that arise with the use of one-loop perturbative renormalization factors, $B_K(\mu=2 \text{ GeV})=0.628(42)$ has been obtained in the continuum limit in the modified minimal subtraction (MS) scheme with naive dimensional regularization (NDR).

Recent development of the domain wall [7–9] and overlap [10,11] fermion formalisms has opened a prospect toward an even better calculation. Even at finite lattice spacings, these formulations maintain both flavor and chiral symmetries, either of which is broken in the Wilson-type fermion action or the KS quark action. Hence one expects that systematic as well as statistical uncertainties are better controlled in these formulations than others. A pioneering calculation of the B_K parameter in this direction was made in Ref. [12] using the domain wall fermion formalism of QCD (DWQCD). In this article we present results of our study toward a precision determination of B_K with DWQCD.

Our investigation is carried out in the quenched approximation using Shamir's formulation of domain-wall fermion for quarks [9], and a renormalization group (RG) improved gauge action for gluons [13]. The latter choice is motivated by the result [14] that chiral symmetry is much better realized with this action than for the plaquette gauge action. We may also expect that scaling violation in B_K arising from the gauge action is improved with the use of the RG-improved action.

We examine effects due to finite fifth dimensional size N_5 and finite spatial size N_σ in detail. Scaling behavior of B_K is studied by adopting $\beta=2.6$ and 2.9 corresponding to the lattice spacing $a^{-1}\approx 2$ and 3 GeV. Matching to the con-

*Present address: RIKEN BNL Research Center, Brookhaven National Laboratory, Upton, NY 11973.

†Present address: Department of Physics, University of Wales, Swansea SA2 8PP, UK.

‡On leave at Department of Physics, Brookhaven National Laboratory, Upton, NY 11973-5000.

§Present address: CERN, Theory Division, CH-1211 Geneva 23, Switzerland.

||Present address: Department of Biochemistry and Molecular Biology, University College London, London, England, UK.

tinuum operator is made perturbatively at one loop order. Making a constant fit in a for the continuum extrapolation, we obtain $B_K(\mu=2 \text{ GeV})=0.5746(61)(191)$ as an estimate of the continuum value in the $\overline{\text{MS}}$ scheme with naive dimensional regularization (NDR). Here the first error is statistical and the second error is an estimated systematic error due to scaling violation and $\mathcal{O}(\alpha_{\overline{\text{MS}}}^2)$ terms in the renormalization factors. This value is consistent with the Kogut-Susskind result quoted above, albeit lying at the lower edge of the one standard deviation error band of the latter result. We also report on light quark masses obtained from meson mass measurements in our simulation.

This paper is organized as follows. In Sec. II we define the fermion and gluon actions, where we recapitulate the argument for choosing the RG-improved action for gluons. Numerical simulations and run parameters are described in Sec. III. In Sec. IV we discuss the operator matching between the lattice and continuum. Hadron mass results, in particular the chiral behavior of pseudo scalar meson mass, are discussed in Sec. V. Our main results for the kaon B parameter are given in Sec. VI. Section VII is devoted to the derivation of light quark mass. We close the paper with a brief summary and comments in Sec. VIII.

II. ACTION

We employ Shamir's domain-wall fermion action [8,9]. Flipping the sign of the Wilson term and the domain wall height M , we write

$$S_f = - \sum_{x,s,y,s'} \bar{\psi}(x,s) D_{dwf}(x,s;y,s') \psi(y,s') + \sum_x m_f \bar{q}(x) q(x), \quad (2.1)$$

$$D_{dwf}(x,s;y,s') = D^4(x,y) \delta_{s,s'} + D^5(s,s') \delta_{x,y} + (M-5) \delta_{x,y} \delta_{s,s'}, \quad (2.2)$$

$$D^4(x,y) = \sum_{\mu} \frac{1}{2} [(1-\gamma_{\mu}) U_{x,\mu} \delta_{x+\hat{\mu},y} + (1+\gamma_{\mu}) U_{y,\mu}^{\dagger} \delta_{x-\hat{\mu},y}], \quad (2.3)$$

$$D^5(s,s') = \begin{cases} P_L \delta_{2,s'} & (s=1), \\ P_L \delta_{s+1,s'} + P_R \delta_{s-1,s'} & (1 < s < N_5), \\ P_R \delta_{N_5-1,s'} & (s=N_5), \end{cases} \quad (2.4)$$

where x,y are four-dimensional space-time coordinates, and s,s' are fifth-dimensional or "flavor" indices, bounded as $1 \leq s,s' \leq N_5$ with the free boundary condition at both ends (we assume N_5 to be even); $P_{R/L}$ is the projection matrix $P_{R/L} = (1 \pm \gamma_5)/2$, and m_f is the bare quark mass. The four-

quark operator for our calculation is constructed with the 4-dimensional quark field defined on the edges of the fifth dimensional space,

$$q(x) = P_L \psi(x,1) + P_R \psi(x,N_5), \\ \bar{q}(x) = \bar{\psi}(x,N_5) P_L + \bar{\psi}(x,1) P_R. \quad (2.5)$$

For the gauge part of the action we employ the following form in 4 dimensions:

$$S_{\text{gluon}} = \frac{1}{g^2} \left\{ c_0 \sum_{\text{plaquette}} \text{Tr} U_{pl} + c_1 \sum_{\text{rectangle}} \text{Tr} U_{rtg} + c_2 \sum_{\text{chair}} \text{Tr} U_{chr} + c_3 \sum_{\text{parallelogram}} \text{Tr} U_{plg} \right\}, \quad (2.6)$$

where the first term represents the standard plaquette action, and the remaining terms are six-link loops formed by a 1×2 rectangle, a bent 1×2 rectangle (chair) and a 3-dimensional parallelogram. The coefficients c_0, \dots, c_3 satisfy the normalization condition

$$c_0 + 8c_1 + 16c_2 + 8c_3 = 1. \quad (2.7)$$

The RG-improved action of Iwasaki [13] is defined by setting the parameters to $c_0=3.648, c_1=-0.331, c_2=c_3=0$. With this choice of parameters the action is expected to exhibit smooth gauge field fluctuations approximating those in the continuum limit better than with the unimproved plaquette action.

A basic piece of information for our study of B_K with DWQCD is in what range of the coupling constant $\beta = 6/g^2$ and domain wall height M DWQCD realizes exact chiral symmetry in the limit of infinite fifth dimensional size $N_5 \rightarrow \infty$. This point has been examined in a number of recent studies [14,15]. Investigations using the axial vector Ward-Takahashi identity show that a non-zero residual quark mass m_{5q} , which represents chiral symmetry breaking, remains even in the limit of infinite fifth dimensional size $N_5 \rightarrow \infty$ if the lattice spacing is as coarse as $a^{-1} \approx 1 \text{ GeV}$.

The chiral property is much improved as the coupling constant is decreased. In the range corresponding to $a^{-1} \sim 2 \text{ GeV}$, the value of residual quark mass becomes an order of magnitude smaller than at $a^{-1} \sim 1 \text{ GeV}$ at similar fifth dimensional sizes N_5 . For the standard plaquette gauge action, it is still not clear whether m_{5q} vanishes exponentially with a small decay rate [15] or remains finite, albeit very small, as $N_5 \rightarrow \infty$ [14]. In contrast, for the RG-improved gauge action, the residual quark mass shows an N_5 dependence consistent with an exponential decay in N_5 up to $N_5 = 24$. Furthermore the magnitude of m_{5q} is an order of magnitude smaller than that for the plaquette gauge action.

We can conclude that chiral symmetry is much better realized with the RG-improved gauge action than with the plaquette gauge action. We therefore employ the RG-improved gauge action for our investigation of the B_K parameter.

TABLE I. Simulation parameters together with the number of configurations analyzed shown in bold numbers.

β	2.6	2.6	2.6	2.6	2.9	2.9
a^{-1} (GeV)	1.875(56)	1.807(37)	1.758(51)	1.847(43)	2.869(68)	2.807(55)
N_t	40	40	40	40	60	60
N_σ	16	24	24	32	24	32
N_5	16	16	32	16	16	16
$N_\sigma a$ (fm)	1.7	2.6	2.6	3.4	1.7	2.3
# conf.	122	76	50	25	76	50

III. RUN PARAMETERS AND MEASUREMENTS

Parameters of our simulations and the number of configurations employed are summarized in Table I. We carry out runs at two values of coupling, $\beta=2.6$ and 2.9 , corresponding to a lattice spacing $a^{-1}=1.81(4)$ GeV and $2.81(6)$ GeV determined from the ρ meson mass $m_\rho=770$ MeV. The first value is chosen since chiral symmetry is sufficiently well realized [14], and the second value is selected to check scaling violation effects.

For our main runs we use the lattice size $N_\sigma^3 \times N_t \times N_5 = 24^3 \times 40 \times 16$ at $\beta=2.6$, and $32^3 \times 60 \times 16$ at $\beta=2.9$. These lattices have a reasonably large spatial size of $aN_\sigma \approx 2.6$ fm or 2.3 fm respectively. The choice of $N_5=16$ at $\beta=2.6$ is based on our previous result [14] that the anomalous quark mass is already quite small, $m_{5q}=0.274(42)$ MeV, for this parameter set with the domain wall height $M=1.8$. In this paper the domain wall height is also taken to be $M=1.8$.

We examine the dependence on the fifth dimensional length N_5 at $\beta=2.6$ for the spatial size $N_\sigma=24$ using $N_5=16$ and $N_5=32$. Since we expect the decay rate in N_5 to become larger toward weaker coupling, we only employ $N_5=16$ at $\beta=2.9$.

The spatial size dependence is examined at $\beta=2.6$ varying the spatial size from $N_\sigma=24$ to either $N_\sigma=16$ or 32 , which correspond to the physical size of $aN_\sigma \sim 1.7$ and 3.4 fm. The size dependence is also checked at $\beta=2.9$ by adopting $N_\sigma=24$ and 32 ($aN_\sigma=1.7, 2.3$ fm).

We take degenerate quarks in our calculations. The common value of bare quark mass is chosen to be $m_f a = 0.01, 0.02, 0.03, 0.04$ at both $\beta=2.6$ and 2.9 , which covers the range $m_{PS}/m_V \approx 0.4-0.8$.

Quenched gauge configurations are generated on four-dimensional lattices. A sweep of gauge update contains one pseudo-heatbath and four overrelaxation steps. After a thermalization of 2000 sweeps hadron propagators and 3-point functions necessary to evaluate B_K are calculated at every 200th sweep. The gauge configuration on each fifth dimensional coordinate s is identical and is fixed to the Coulomb gauge.

In the course of our simulation we measure the kaon B parameter,

$$B_K = \frac{\langle K | \bar{s} \gamma_\mu (1 - \gamma_5) d \bar{s} \gamma_\mu (1 - \gamma_5) d | K \rangle}{\frac{8}{3} \langle K | \bar{s} \gamma_\mu \gamma_5 d | 0 \rangle \langle 0 | \bar{s} \gamma_\mu \gamma_5 d | K \rangle} \quad (3.1)$$

and the matrix element divided by the pseudo scalar density,

$$B_P = \frac{\langle K | \bar{s} \gamma_\mu (1 - \gamma_5) d \bar{s} \gamma_\mu (1 - \gamma_5) d | K \rangle}{\langle K | \bar{s} \gamma_5 d | 0 \rangle \langle 0 | \bar{s} \gamma_5 d | K \rangle} \quad (3.2)$$

which should vanish at $m_\pi \rightarrow 0$. The s and d quark fields defining these quantities are the boundary fields given by Eq. (2.5), and the four-quark and bilinear operators are taken to be local in the 4-dimensional space-time.

The domain-wall quark propagator needed to extract the B parameters above is calculated with the conjugate gradient algorithm with an even-odd pre-conditioning. Two quark propagators are evaluated for each configuration corresponding to the wall source placed at either $t=1$ or 40 at $\beta=2.6$ ($t=4$ or 57 at $\beta=2.9$) in the time direction with the Dirichlet boundary condition, while the periodic boundary condition is imposed in the spatial directions. The two quark propagators are combined to form the kaon Green's function with an insertion of the four-quark operator at time slices $1 \leq t \leq N_t$ in a standard manner (see, e.g., Ref. [6]).

We employ the quark propagators above to also evaluate pseudo scalar and vector meson propagators, and extract their masses. These masses are calculated for degenerate quark-antiquark pair. The physical point for light quark masses m_{ud} and m_s is calculated by linearly fitting the meson masses m_{PS}^2 and m_V as a function of m_f , and using the experimental values of m_π/m_ρ and m_K/m_ρ or m_ϕ/m_ρ as input.

IV. OPERATOR MATCHING

We carry out matching of the lattice and continuum operators at a scale $q^*=1/a$ using one-loop perturbation theory [16] and the $\overline{\text{MS}}$ scheme with NDR in the continuum. The continuum value at a physical scale e.g., $\mu=2$ GeV, is obtained *via* a renormalization group running from $q^*=1/a$ to μ :

TABLE II. Finite parts of the renormalization factors with RG improved gauge action. The mean field approximation is used for the factors at $M=1.4198$ and 1.4687 . Errors from the numerical integration are in the last written digit.

M	z_2	z_m	z_w	z_A	z_P	z_{O_4}
1.8	-3.824	13.148	-25.1295	-9.190	-13.148	-23.868

M	z_2^{MF}	z_m^{MF}	z_w^{MF}	z_A^{MF}	z_P^{MF}	$z_{O_4}^{\text{MF}}$
1.4198	0.651	6.044	-7.92355	-4.692	-6.044	-13.612
1.4687	0.632	6.319	-7.95874	-4.714	-6.319	-13.500

$$\begin{aligned}
B_K(\text{NDR}, \mu) &= \left[1 - \frac{\alpha_{\overline{\text{MS}}}(\mu)}{4\pi} \frac{\gamma_1 \beta_0 - \gamma_0 \beta_1}{2\beta_0^2} \right]^{-1} \\
&\times \left[1 - \frac{\alpha_{\overline{\text{MS}}}(q^*)}{4\pi} \frac{\gamma_1 \beta_0 - \gamma_0 \beta_1}{2\beta_0^2} \right] \\
&\times \left[\frac{\alpha_{\overline{\text{MS}}}(q^*)}{\alpha_{\overline{\text{MS}}}(\mu)} \right]^{-\gamma_0/2\beta_0} B_K(\text{NDR}, q^*), \quad (4.1)
\end{aligned}$$

where $\beta_0=11$, $\beta_1=102$, $\gamma_0=4$ and $\gamma_1=-7$ [17] are the $N_f=0$ quenched values for the renormalization group coefficients.

In the domain wall formalism the renormalization factor of an n -quark operator O_n has a generic form

$$\overline{O_n^{\text{MS}}}(\mu) = Z O_n^{\text{lattice}}(1/a), \quad (4.2)$$

$$Z = (1 - w_0^2)^{-n/2} Z_w^{-n/2} Z_{O_n}, \quad (4.3)$$

where $w_0 = 1 - M$, and Z_w represents the quantum correction to the normalization factor $1 - w_0^2$ of physical quark fields q , \bar{q} , and Z_{O_n} is the vertex correction to O_n . In the present paper we need the factors Z_2 , Z_m , Z_A , Z_P and Z_{O_4} for the quark wave function, quark mass, axial vector current, pseudo scalar density and the four-quark $\Delta S=2$ weak operator. Perturbative calculation of these renormalization factors at one loop order is given in Ref. [16] for the DWQCD system with the standard plaquette gauge action. Here we summarize results for the RG-improved gauge action.

The generic form of the one-loop renormalization factors is given by

$$Z_w(\mu a) = 1 + \frac{2w_0}{1-w_0^2} \frac{g^2 C_F}{16\pi^2} z_w(M), \quad (4.4)$$

$$Z_2(\mu a) = 1 + \frac{g^2 C_F}{16\pi^2} [-\log(\mu a)^2 + z_2(M)], \quad (4.5)$$

$$Z_m(\mu a) = 1 + \frac{g^2 C_F}{16\pi^2} [-3 \log(\mu a)^2 + z_m(M)], \quad (4.6)$$

$$Z_A(\mu a) = 1 + \frac{g^2 C_F}{16\pi^2} z_A(M), \quad (4.7)$$

$$Z_P(\mu a) = 1 + \frac{g^2 C_F}{16\pi^2} [3 \log(\mu a)^2 + z_P(M)], \quad (4.8)$$

$$Z_{O_4}(\mu a) = 1 + \frac{g^2}{16\pi^2} [-2 \log(\mu a)^2 + z_{O_4}(M)], \quad (4.9)$$

where C_F is the second Casimir invariant $C_F=4/3$ and the finite part z_{O_n} is a function of the domain-wall height M . The difference between the plaquette and the RG action resides in the finite part.

In the first row of Table II we list the finite parts of the renormalization factors at $M=1.8$. The one-loop correction in Z_w is very large for our choice of M because of the tadpole factor in z_w and division with $1 - w_0^2$ [16]. Hence we apply a tadpole improvement by explicitly moving the one-loop correction to the domain wall height M from Z_w to w_0 additively, and by factoring out a tadpole factor $u^{n/2} = P^{n/8}$ with P the plaquette from Z_{O_n} . This leads to the rewriting,

$$Z \rightarrow Z^{\text{MF}} = (1 - (w_0^{\text{MF}})^2)^{-n/2} (Z_w^{\text{MF}})^{-n/2} u^{n/2} Z_{O_n}^{\text{MF}}, \quad (4.10)$$

where

$$w_0^{\text{MF}} = w_0 + 4(1 - u), \quad (4.11)$$

$$Z_w^{\text{MF}} = Z_w|_{w_0=w_0^{\text{MF}}} + \frac{4w_0^{\text{MF}}}{1 - (w_0^{\text{MF}})^2} g^2 C_F u_1, \quad (4.12)$$

$$Z_2^{\text{MF}} = Z_2|_{w_0=w_0^{\text{MF}}} + \frac{1}{2} g^2 C_F u_1, \quad (4.13)$$

$$Z_m^{\text{MF}} = Z_m|_{w_0=w_0^{\text{MF}}} - \frac{1}{2} g^2 C_F u_1, \quad (4.14)$$

$$Z_{O_n}^{\text{MF}} = Z_{O_n}|_{w_0=w_0^{\text{MF}}} + \frac{n}{4} g^2 C_F u_1. \quad (4.15)$$

Here u_1 is the one-loop correction to the tadpole factor $u = 1 - g^2 C_F u_1/2 + \dots$ which has the values

$$u_1 = \begin{cases} 0.125000 & \text{(plaquette action),} \\ 0.052567 & \text{(RG improved action).} \end{cases} \quad (4.16)$$

For the tadpole factor $u = P^{1/4}$ we use the following value of the plaquette for the RG action

$$P = \begin{cases} 0.670632(10) & \text{at } \beta=2.6, \\ 0.707662(5) & \text{at } \beta=2.9 \end{cases} \quad (4.17)$$

obtained from our main simulations. The domain-wall height is shifted according to Eq. (4.11) as

$$M = 1.8 \rightarrow M^{\text{MF}} = \begin{cases} 1.4198 & \text{for } \beta=2.6, \\ 1.4687 & \text{for } \beta=2.9. \end{cases} \quad (4.18)$$

In the second and third rows of Table II we list the finite parts of the renormalization factors after tadpole improvement.

A mean-field estimate appropriate for the RG-improved action is used for calculating the coupling constant $g_2^{\overline{\text{MS}}}(\mu)$, which is given with the following formula for the quenched case [25]

$$\frac{1}{g_2^{\overline{\text{MS}}}(\mu)} = (3.648P - 2.648R) \frac{\beta}{6} + \frac{22}{16\pi^2} \log(\mu a) - 0.1006, \quad (4.19)$$

where R is a 1×2 rectangular Wilson loop whose value is given as

$$R = \begin{cases} 0.45283(2) & \text{at } \beta=2.6, \\ 0.50654(1) & \text{at } \beta=2.9. \end{cases} \quad (4.20)$$

The gauge coupling at $\mu = 1/a$ turns out to be

$$g_2^{\overline{\text{MS}}}(1/a) = \begin{cases} 2.2731 & \text{at } \beta=2.6, \\ 2.0046 & \text{at } \beta=2.9. \end{cases} \quad (4.21)$$

For B_K the factor $(1 - w_0^2)^2 Z_w^2$ cancels out, and the one-loop value is given by the ratio

$$\begin{aligned} Z_{B_K}(\mu a) &= \frac{Z_{O_4}}{Z_A^2} = \frac{1 + (-2 \log(\mu a)^2 + z_{O_4}) g^2 / (16\pi^2)}{(1 + (C_{Fz_A}) g^2 / (16\pi^2))^2} \\ &= 1 + \frac{g^2}{16\pi^2} (-2 \log(\mu a)^2 + z_{B_K}). \end{aligned} \quad (4.22)$$

In Table III we give the finite parts of Z_{B_K} with and without mean field approximation at $M = 1.8$ together with those for Z_{B_P} ,

$$Z_{B_P}(\mu a) = 1 + \frac{g^2}{16\pi^2} (-10 \log(\mu a)^2 + z_{B_P}). \quad (4.23)$$

The finite parts z_{O_4} and $2C_{Fz_A}$ are very similar in magnitude, albeit individually not very small. As a result the

TABLE III. Finite parts of the renormalization factors z_{B_K} and z_{B_P} with RG improved gauge action. The mean field approximation is used for z_{B_P} at $M = 1.4198$ and 1.4687 , while the effect of the approximation on z_{B_K} is just to shift the domain-wall height. Errors from the numerical integration are in the last written digit.

M	z_{B_K}	z_{B_P}	$z_{B_P}^{\text{MF}}$
1.8	0.64	11.19	—
1.4198	—1.10	—	2.51
1.4687	—0.93	—	3.35

finite part $z_{B_K} = z_{O_4} - 2C_{Fz_A}$ for B_K is small, and the renormalization factor for B_K with the tadpole improvement turned out to be very near unity, e.g., at the matching scale $q^* = 1/a$,

$$\overline{Z_{B_K}^{\text{MS}}}(q^* = 1/a) = \begin{cases} 0.984 & \text{at } \beta=2.6, \\ 0.988 & \text{at } \beta=2.9. \end{cases} \quad (4.24)$$

The Z factor at the scale $\mu = 2$ GeV obtained with a 2-loop running with Eq. (4.1) [17] becomes

$$\overline{Z_{B_K}^{\text{MS}}}(\mu = 2 \text{ GeV}) = \begin{cases} 0.979 & \text{at } \beta=2.6, \\ 1.006 & \text{at } \beta=2.9. \end{cases} \quad (4.25)$$

Meanwhile Z_{B_P} is evaluated by setting $\mu = 2$ GeV in Eq. (4.23)

$$\overline{Z_{B_P}^{\text{MS}}}(\mu = 2 \text{ GeV}) = \begin{cases} 1.007 & \text{at } \beta=2.6, \\ 1.129 & \text{at } \beta=2.9. \end{cases} \quad (4.26)$$

For quark mass the renormalization factor at the matching scale $q^* = 1/a$ takes the values

$$\begin{aligned} \overline{Z_q^{\text{MS}}}(q^* = 1/a) &= (1 - (w_0^{\text{MF}})^2) (Z_w^{\text{MF}}) u^{-1} Z_m^{\text{MF}}(q^* = 1/a) \\ &= \begin{cases} 1.173371 & \text{at } \beta=2.6, \\ 1.094189 & \text{at } \beta=2.9. \end{cases} \end{aligned} \quad (4.27)$$

With a renormalization group running from the scale q^* to $\mu = 2$ GeV using the four-loop anomalous dimension and beta function [18], we have

$$m(\mu) = \frac{c(\alpha_{\overline{\text{MS}}}(\mu)/\pi)}{c(\alpha_{\overline{\text{MS}}}(q^*)/\pi)} m(q^*), \quad (4.28)$$

and the renormalization factor becomes

$$\overline{Z_q^{\text{MS}}}(\mu = 2 \text{ GeV}) = \begin{cases} 1.155769 & \text{at } \beta=2.6, \\ 1.147224 & \text{at } \beta=2.9. \end{cases} \quad (4.29)$$

The four-loop running factor $c(\alpha_{\overline{\text{MS}}}(\mu)/\pi)$ is given by [18]

$$\begin{aligned}
c(x) = & (x)^{\bar{\gamma}_0} \{ 1 + (\bar{\gamma}_1 - \bar{\beta}_1 \bar{\gamma}_0)x + \frac{1}{2} [(\bar{\gamma}_1 - \bar{\beta}_1 \bar{\gamma}_0)^2 + \bar{\gamma}_2 + \bar{\beta}_1^2 \bar{\gamma}_0 \\
& - \bar{\beta}_1 \bar{\gamma}_1 - \bar{\beta}_2 \bar{\gamma}_0] x^2 + [\frac{1}{6} (\bar{\gamma}_1 - \bar{\beta}_1 \bar{\gamma}_0)^3 + \frac{1}{2} (\bar{\gamma}_1 - \bar{\beta}_1 \bar{\gamma}_0) \\
& \times (\bar{\gamma}_2 + \bar{\beta}_1^2 \bar{\gamma}_0 - \bar{\beta}_1 \bar{\gamma}_1 - \bar{\beta}_2 \bar{\gamma}_0) + \frac{1}{3} (\bar{\gamma}_3 - \bar{\beta}_1^3 \bar{\gamma}_0 \\
& + 2 \bar{\beta}_1 \bar{\beta}_2 \bar{\gamma}_0 - \bar{\beta}_3 \bar{\gamma}_0 + \bar{\beta}_1 \bar{\gamma}_1 - \bar{\beta}_2 \bar{\gamma}_1 - \bar{\beta}_1 \bar{\gamma}_2)] x^3 \\
& + \mathcal{O}(x^4) \}, \quad (4.30)
\end{aligned}$$

where

$$\bar{\gamma}_i = \frac{\gamma_i^m}{4^i \beta_0}, \quad \bar{\beta}_i = \frac{\beta_i}{4^i \beta_0}, \quad (4.31)$$

$$\beta_0 = 11, \quad \beta_1 = 102, \quad \beta_2 = \frac{2857}{2},$$

$$\beta_3 = \frac{149753}{6} + 3564 \zeta(3), \quad (4.32)$$

$$\gamma_0^m = 4, \quad \gamma_1^m = \frac{202}{3}, \quad \gamma_2^m = 1249, \quad (4.33)$$

$$\gamma_3^m = \frac{4603055}{162} + \frac{135680}{27} \zeta(3) - 8800 \zeta(5) \quad (4.34)$$

with ζ the Riemann zeta-function.

Let us add a comment on the systematic error due to operator matching. Since we have used the one-loop renormalization factor for operator matching, the systematic error should include contributions from higher loop corrections. We estimate the magnitude of these corrections by changing the matching scale from $q^* = 1/a$ to $q^* = \pi/a$ and also adopting a different definition for gauge coupling using the plaquette value only [25] given by

$$\frac{1}{g_{\overline{\text{MS}}}^2(\mu)} = P \frac{\beta}{6} + \frac{22}{16\pi^2} \log(\mu a) + 0.2402. \quad (4.35)$$

The gauge coupling at $\mu = 1/a$ becomes

$$g_{\overline{\text{MS}}}^2(1/a) = \begin{cases} 1.8839 & \text{at } \beta = 2.6, \\ 1.7176 & \text{at } \beta = 2.9. \end{cases} \quad (4.36)$$

V. PSEUDO SCALAR AND VECTOR MESON MASSES

A. Extraction of meson masses

We extract pseudo scalar and vector meson masses m_{PS} and m_V at each m_f , N_σ and N_5 by a single exponential fit of

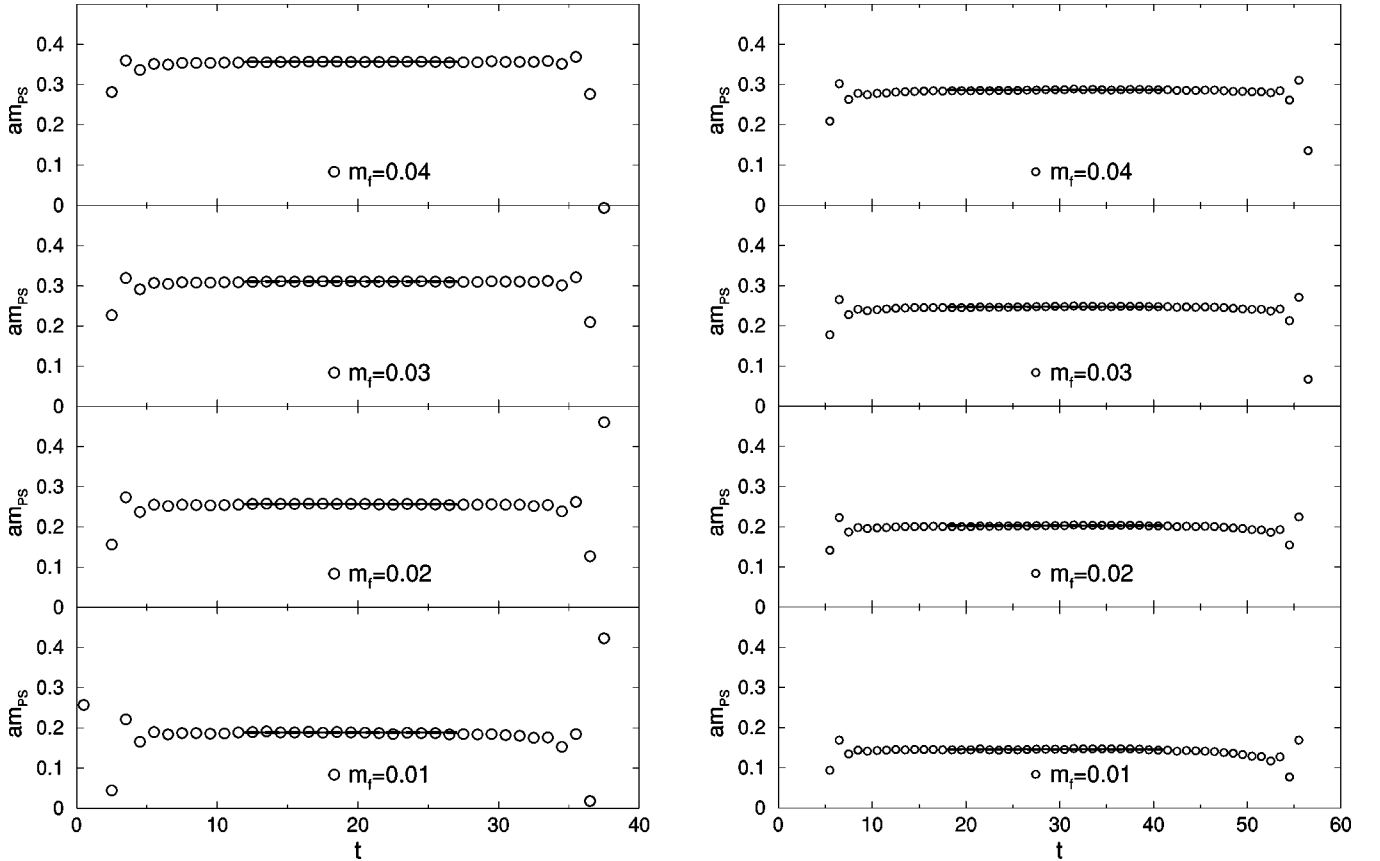


FIG. 1. Effective pseudo scalar meson mass as a function of temporal distance t at $\beta = 2.6$ on a $24^3 \times 40 \times 16$ lattice (left) and at $\beta = 2.9$ on a $32^3 \times 60 \times 16$ lattice (right). Lines show constant fit over the fitted range.

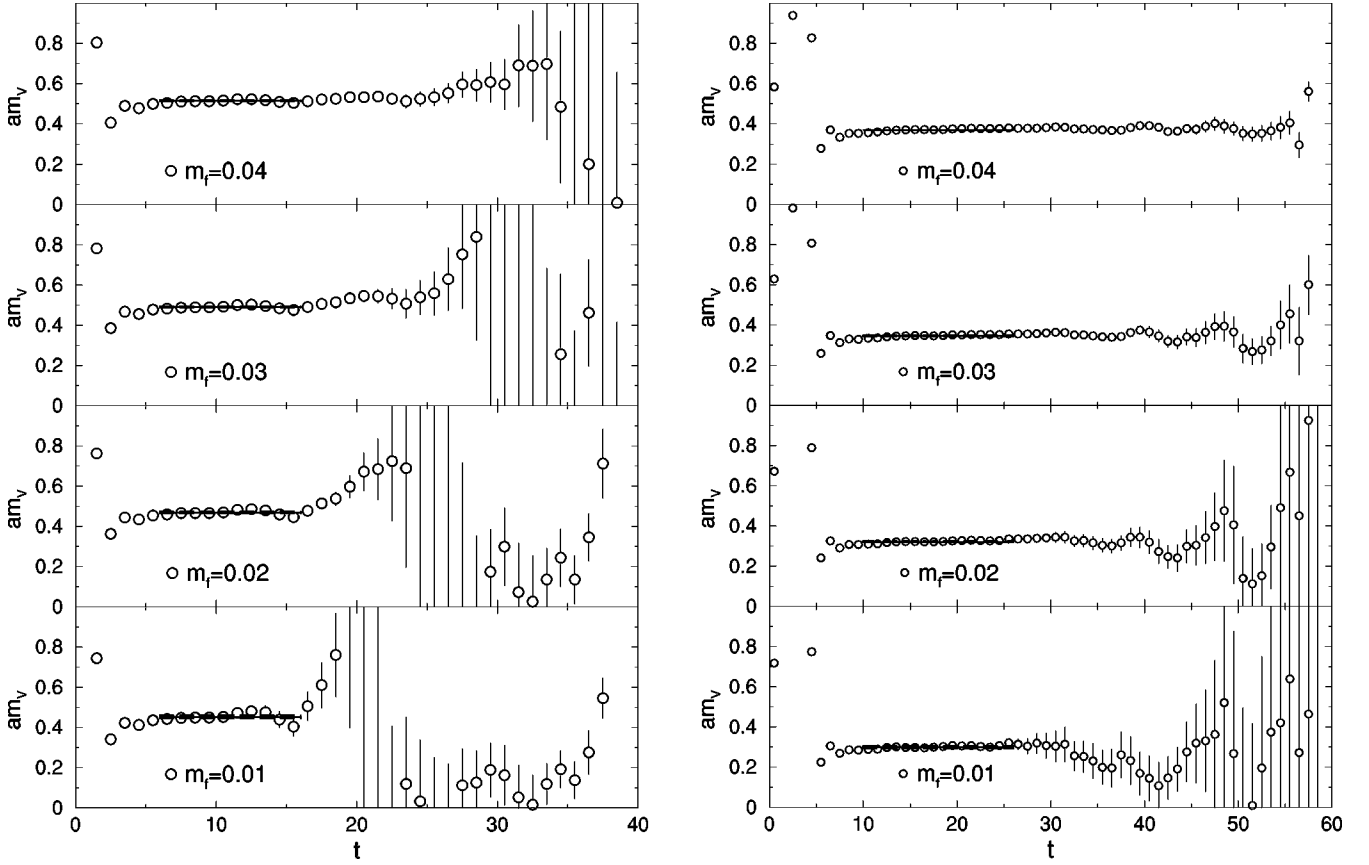


FIG. 2. Effective vector meson mass as a function of temporal distance t at $\beta=2.6$ on a $24^3 \times 40 \times 16$ lattice (left) and at $\beta=2.9$ on a $32^3 \times 60 \times 16$ lattice (right). Lines show constant fit over the fitted range.

meson propagators. Representative plots of effective mass are shown in Figs. 1 and 2. The fitting range chosen from inspection of such plots is $12 \leq t \leq 27$ and $6 \leq t \leq 16$ for pseudo scalar and vector meson mass for all simulations at $\beta=2.6$, and $18 \leq t \leq 41$ and $10 \leq t \leq 26$ at $\beta=2.9$. In Tables IV–IX we list the numerical values of $m_{PS}a$, m_Va and the ratio at four quark masses $m_f a = 0.01, 0.02, 0.03, 0.04$ for each set of run parameter. The errors given are calculated by a single elimination jackknife procedure.

B. Chiral extrapolation

For chiral extrapolation we fit the light hadron masses m_{PS}^2 and m_V linearly as a function of $m_f a$ as illustrated in Figs. 3 and 4. Since pseudo scalar meson mass thus extrapolated does not vanish at $m_f=0$, we employ a fit of the form

$$m_{PS}^2 a^2 = A_{PS}(m_f a + m_{\text{res(fs)}} a), \quad (5.1)$$

$$m_V a = A_V + B_V m_f a \quad (5.2)$$

and determine the parameters $A_{PS}, m_{\text{res(fs)}} a$ for the pseudo scalar meson, and A_V, B_V for the vector meson. The suffix (fs) in $m_{\text{res(fs)}} a$ is added since non-zero values of m_{PS} at $m_f = 0$ represents effects of finite spatial size as discussed below in Sec. V C. Some details of fits are described in the Appendix. The physical point for the bare quark mass parameter m_f corresponding to physical u and d quark (m_f^{ud}), which are assumed degenerate, and s quark (m_f^s) are fixed by the equations

TABLE IV. Data for B_K , B_P , m_{PS} , m_V , and m_{PS}/m_V at each quark mass m_f at $\beta=2.6$ on $16^3 \times 40 \times 16$ lattice.

$\beta=2.6$ on $16^3 \times 40 \times 16$ lattice					
m_f	B_K	B_P	m_{PS}	m_V	m_{PS}/m_V
0.01	0.487(19)	0.0225(10)	0.1902(29)	0.438(12)	0.434(13)
0.02	0.566(14)	0.0569(14)	0.2554(23)	0.4639(72)	0.5505(97)
0.03	0.615(11)	0.0945(17)	0.3083(21)	0.4904(54)	0.6287(80)
0.04	0.6486(85)	0.1327(19)	0.3548(20)	0.5168(43)	0.6865(69)

TABLE V. Data for B_K , B_P , m_{PS} , m_V , and m_{PS}/m_V at each quark mass m_f at $\beta=2.6$ on $24^3 \times 40 \times 16$ lattice.

$\beta=2.6$ on $24^3 \times 40 \times 16$ lattice					
m_f	B_K	B_P	m_{PS}	m_V	m_{PS}/m_V
0.01	0.5196(69)	0.02487(38)	0.1883(13)	0.4522(83)	0.4164(80)
0.02	0.5769(47)	0.05777(55)	0.2567(12)	0.4683(51)	0.5481(65)
0.03	0.6155(42)	0.09367(70)	0.3102(11)	0.4900(36)	0.6331(52)
0.04	0.6453(39)	0.13092(83)	0.35647(97)	0.5141(29)	0.6934(42)

TABLE VI. Data for B_K , B_P , m_{PS} , m_V , and m_{PS}/m_V at each quark mass m_f at $\beta=2.6$ on $24^3 \times 40 \times 32$ lattice.

$\beta=2.6$ on $24^3 \times 40 \times 32$ lattice					
m_f	B_K	B_P	m_{PS}	m_V	m_{PS}/m_V
0.01	0.5225(89)	0.02444(47)	0.1874(16)	0.463(12)	0.405(11)
0.02	0.5780(63)	0.05751(71)	0.2558(14)	0.4760(73)	0.5374(89)
0.03	0.6152(54)	0.09329(90)	0.3093(12)	0.4956(50)	0.6242(67)
0.04	0.6437(49)	0.1302(10)	0.3556(11)	0.5182(37)	0.6862(53)

TABLE VII. Data for B_K , B_P , m_{PS} , m_V , and m_{PS}/m_V at each quark mass m_f at $\beta=2.6$ on $32^3 \times 40 \times 16$ lattice.

$\beta=2.6$ on $32^3 \times 40 \times 16$ lattice					
m_f	B_K	B_P	m_{PS}	m_V	m_{PS}/m_V
0.01	0.5260(47)	0.02594(33)	0.1841(13)	0.4424(92)	0.4161(86)
0.02	0.5766(40)	0.05873(51)	0.2535(12)	0.4608(59)	0.5501(77)
0.03	0.6124(39)	0.09460(72)	0.3076(12)	0.4847(44)	0.6347(66)
0.04	0.6424(35)	0.13196(88)	0.3544(11)	0.5097(36)	0.6954(57)

TABLE VIII. Data for B_K , B_P , m_{PS} , m_V , and m_{PS}/m_V at each quark mass m_f at $\beta=2.9$ on $24^3 \times 60 \times 16$ lattice.

$\beta=2.9$ on $24^3 \times 60 \times 16$ lattice					
m_f	B_K	B_P	m_{PS}	m_V	m_{PS}/m_V
0.01	0.512(18)	0.0340(14)	0.1444(20)	0.2915(59)	0.496(13)
0.02	0.591(11)	0.0802(17)	0.2007(17)	0.3172(40)	0.6328(96)
0.03	0.6403(84)	0.1295(21)	0.2460(15)	0.3425(32)	0.7182(78)
0.04	0.6758(75)	0.1793(24)	0.2856(14)	0.3681(27)	0.7760(65)

TABLE IX. Data for B_K , B_P , m_{PS} , m_V , and m_{PS}/m_V at each quark mass m_f at $\beta=2.9$ on $32^3 \times 60 \times 16$ lattice.

$\beta=2.9$ on $32^3 \times 60 \times 16$ lattice					
m_f	B_K	B_P	m_{PS}	m_V	m_{PS}/m_V
0.01	0.5318(72)	0.03412(64)	0.1459(12)	0.2984(54)	0.489(10)
0.02	0.5922(58)	0.07885(97)	0.2022(12)	0.3209(31)	0.6302(78)
0.03	0.6345(51)	0.1271(12)	0.2470(12)	0.3451(23)	0.7157(65)
0.04	0.6669(46)	0.1761(14)	0.2863(11)	0.3700(19)	0.7738(55)

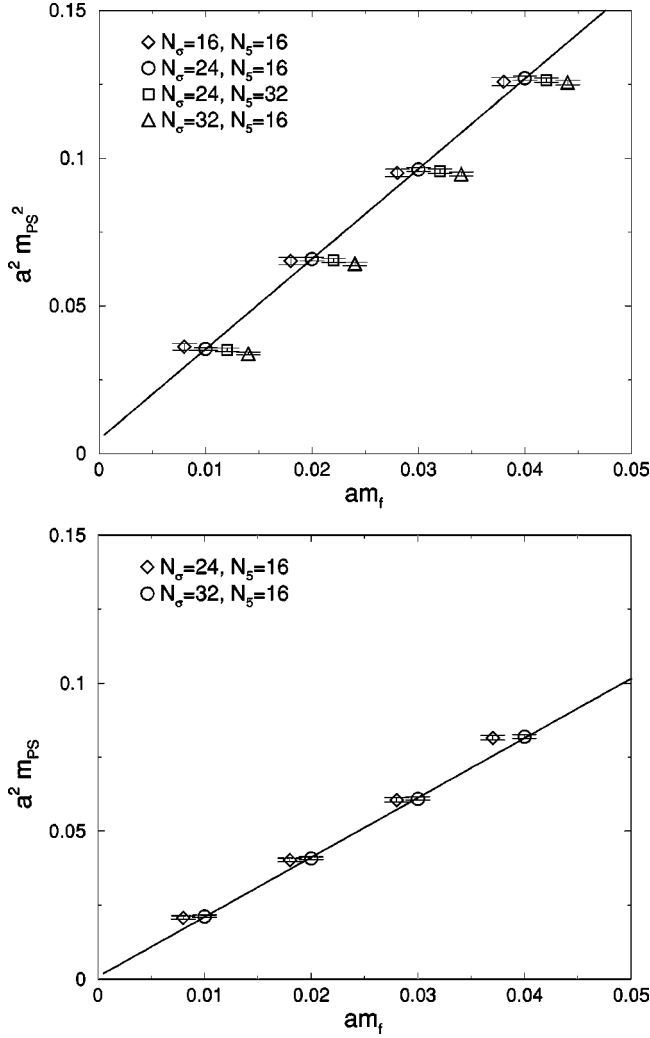


FIG. 3. Pseudo scalar meson mass squared as a function of bare quark mass m_f at $\beta=2.6$ (top) and at $\beta=2.9$ (bottom). Lines show linear fits to main runs. The data except for the main run are shifted in m_f .

$$\frac{\sqrt{A_{PS}(m_f^{ud}a + m_{\text{res(fs)}}a)}}{A_V + B_V m_f^{ud}a} = \frac{m_\pi}{m_\rho} = \frac{0.135}{0.77}, \quad (5.3)$$

$$\frac{\sqrt{A_{PS}(m_f^s a/2 + m_{\text{res(fs)}}a)}}{A_V + B_V m_f^{ud}a} = \frac{m_K}{m_\rho} = \frac{0.495}{0.77}, \quad (5.4)$$

$$\frac{A_V + B_V m_f^s(\phi)a}{A_V + B_V m_f^{ud}a} = \frac{m_\phi}{m_\rho} = \frac{1.0194}{0.77}, \quad (5.5)$$

where for s quark we employ the kaon (m_f^s) or phi ($m_f^s(\phi)$) meson mass as input. We then fix the lattice spacing a by setting the vector meson mass at the physical quark mass point m_f^{ud} to the experimental value $m_\rho = 770$ MeV. Numerical values of lattice spacing and other parameters are listed in Table X.

In Fig. 5 we plot results for $m_\rho a$ at the physical point. The values for given β are reasonably consistent with each other;

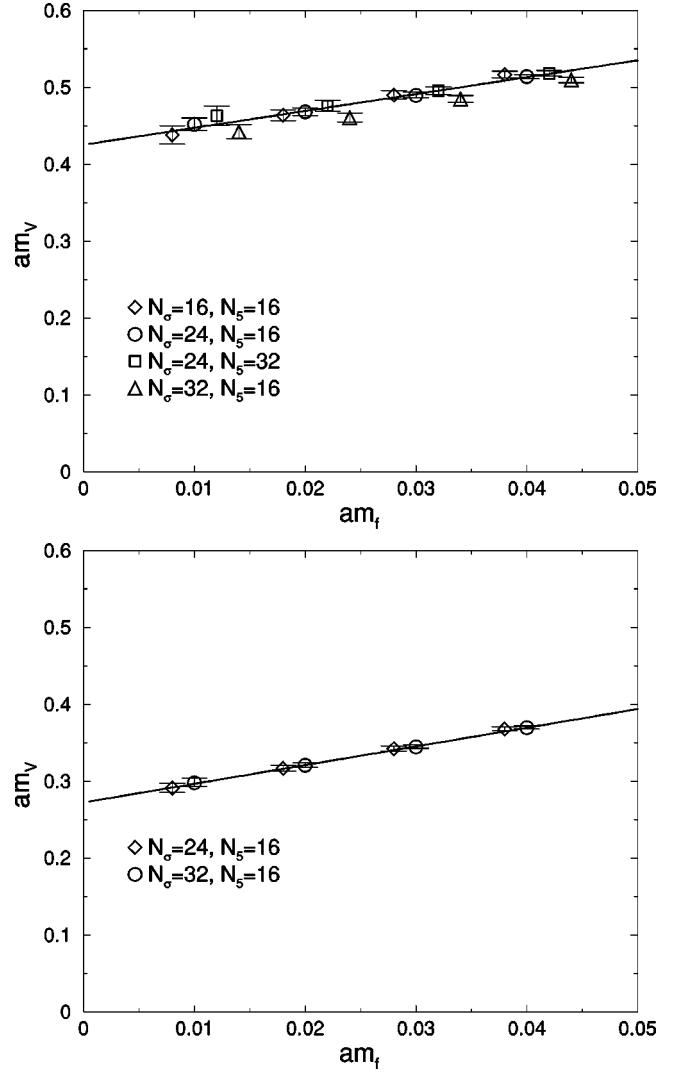


FIG. 4. Vector meson mass as a function of bare quark mass m_f at $\beta=2.6$ (top) and at $\beta=2.9$ (bottom). Lines show linear fits to main runs. The data except for the main run are shifted in m_f .

the variation of results depending on spatial volume is mild, and the difference between the fifth dimensional size $N_5 = 16$ and 32 at $\beta=2.6$ on $24^3 \times 40$ lattice is a one-standard deviation effect. In the following analyses we use the lattice spacing corresponding to each spatial size and fifth dimensional length.

C. Chiral property of pseudo scalar meson mass

We have already mentioned that the pseudo scalar meson mass, if linearly extrapolated, does not vanish at $m_f=0$. We have also examined alternative fits including either a quadratic term, $(m_f a)^2$, or a quenched chiral logarithm term, $m_f a \log(m_f a)$, in addition to the linear term. We have found that these yield almost identical values of the pseudo scalar meson mass at $m_f=0$ as is shown in the Appendix in more detail. We observe from the results at $\beta=2.6$ shown in the left panel of Fig. 3 that the non-zero pseudo scalar meson mass cannot be explained as an effect of finite fifth dimensional lengths, since the data at $N_5=16$ (open circles) and

TABLE X. Results of meson mass fits.

β	2.6	2.6	2.6	2.6	2.9	2.9
N_t	40	40	40	40	60	60
N_σ	16	24	24	32	24	32
N_5	16	16	32	16	16	16
$a^{-1}(\text{GeV})$	1.875(56)	1.807(37)	1.758(51)	1.847(43)	2.869(68)	2.807(55)
$m_V(m_f=0)a$	0.411(12)	0.4261(87)	0.438(13)	0.4169(97)	0.2684(64)	0.2743(54)
$m_{PS}^2(m_f=0)a^2$	0.0060(12)	0.00490(53)	0.00467(69)	0.00330(52)	0.00038(62)	0.00099(34)
$m_{\text{res(fs)}}a$	0.00201(42)	0.00161(18)	0.00153(23)	0.00108(17)	0.00019(31)	0.00049(17)
$m_{\text{res(fs)}}(\text{MeV})$	3.77(78)	2.90(32)	2.70(42)	1.99(32)	0.54(89)	1.38(48)
$m_f^{ud}a$	-0.00027(41)	0.00022(19)	0.00040(26)	0.00067(18)	0.00091(32)	0.00066(18)
$m_f^s a/2(K)$	0.0216(15)	0.0233(10)	0.0248(15)	0.0227(11)	0.01475(82)	0.01515(70)
$m_f^s a(\phi)$	0.0503(62)	0.0632(64)	0.071(11)	0.0583(59)	0.0350(25)	0.0373(25)

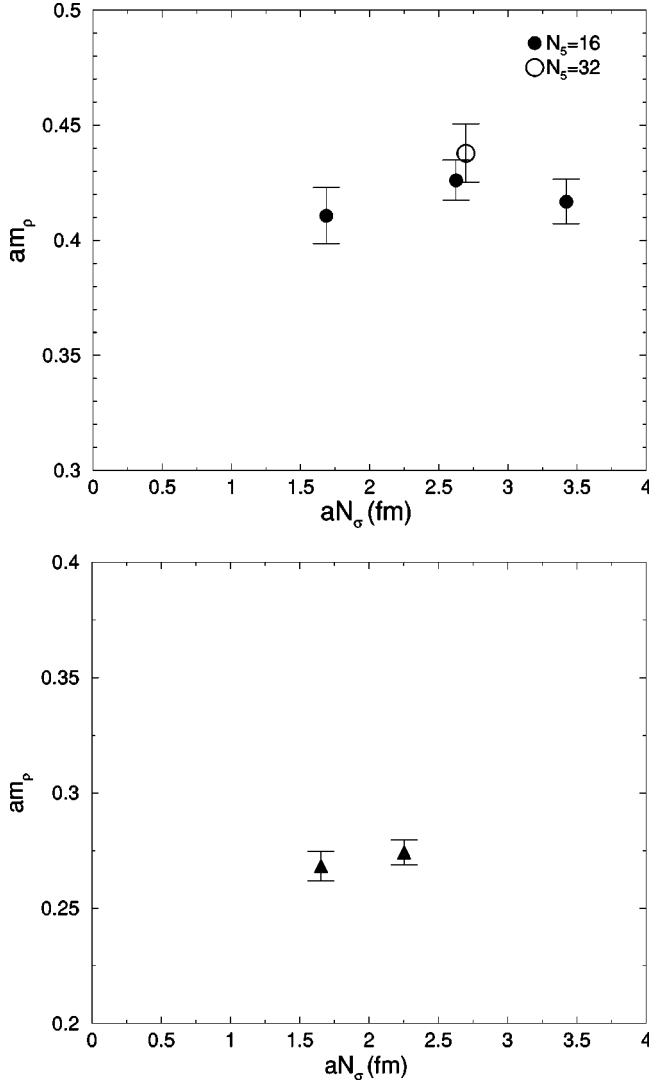


FIG. 5. Rho meson mass as a function of spatial lattice size N_σ at $\beta=2.6$ (top) and at $\beta=2.9$ (bottom). Filled symbols represent data at fifth dimensional length $N_5=16$ and an open circle represents that at $N_5=32$.

$N_5=32$ (open squares) are consistent within the error down to the smallest quark mass $m_f a=0.01$. This conclusion is also supported by an analysis of the anomalous quark mass m_{5q} defined by the axial Ward-Takahashi identity [14]. This quantity provides a measure of chiral symmetry breaking due to a finite N_5 . It was found that m_{5q} has only a very small value of $m_{5q}=0.274(42)$ MeV for $N_5=16$ at $\beta=2.6$. For comparison, the magnitude of $m_{\text{res(fs)}}$ obtained from the linear fit is 2–4 MeV as one can see from Table X.

Examining the spatial size dependence of results at $\beta=2.6$ (left panel of Fig. 3) for $N_\sigma=16, 24$ and 32, we observe that the three points are mutually consistent within the errors for the heavier quark mass of $m_f a=0.04, 0.03$ and 0.02, but that they show a decrease toward larger spatial volumes at our lightest quark mass $m_f a=0.01$. This indicates that the non-zero pseudo scalar meson mass at $m_f=0$ in the linear extrapolation reflects a finite spatial volume effects in our pseudo scalar meson mass data.

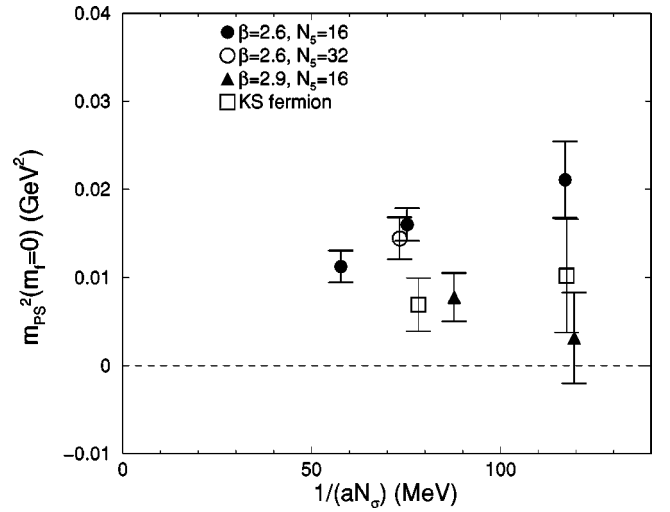


FIG. 6. Pseudo scalar meson mass at $m_f=0$ as a function of spatial lattice size N_σ . Filled symbols represent data at fifth dimensional length $N_5=16$ and an open circle represents that at $N_5=32$. The results of the KS fermion at similar volume size [19] is also plotted with open squares for comparison.

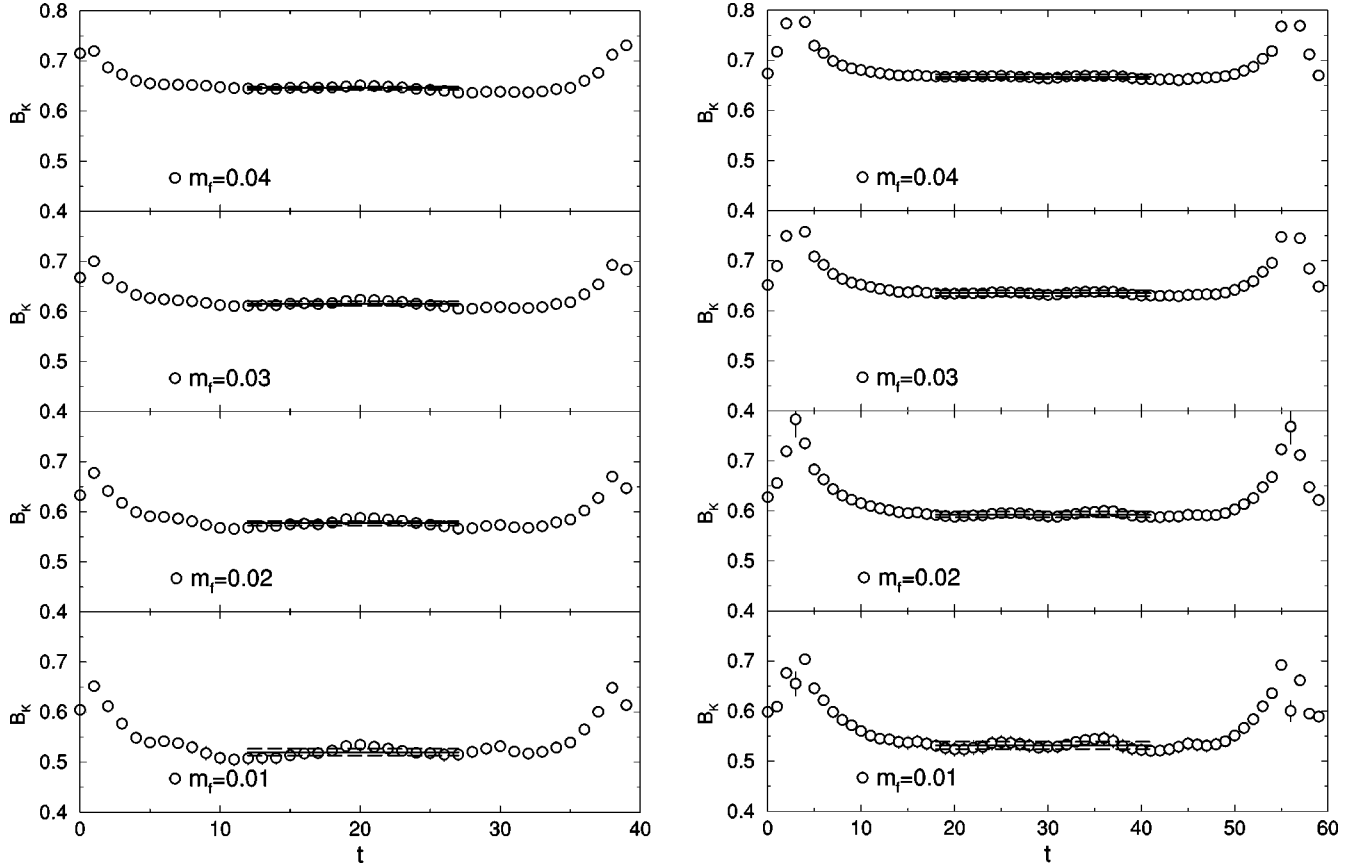


FIG. 7. Ratio of weak matrix element with vacuum saturation (3.1) as a function of temporal distance t at $\beta=2.6$ on a $24^3 \times 40 \times 16$ lattice (left) and at $\beta=2.9$ on a $32^3 \times 60 \times 16$ lattice (right). Lines show constant fit over the fitted range.

To make this point explicit, we plot the values of m_{PS}^2 at $m_f=0$ as a function $1/N_\sigma a$ in Fig. 6. At $\beta=2.6$ the results (filled circles) exhibit a decrease as $1/N_\sigma a \rightarrow 0$. For comparison we plot by open squares results for the Kogut-Susskind quark action, which retains $U(1)$ chiral symmetry, obtained at a similar lattice spacing of $a^{-1} \approx 2$ GeV and spatial lattice sizes of $N_\sigma \approx 16-24$ [19]. A similar magnitude of m_{PS}^2 in the chiral limit between the two quark actions both having chiral symmetry corroborates finite-size effects as the origin of non-zero values m_{PS}^2 .

The two points for $\beta=2.9$ do not show a clear volume dependence. This reflects an absence of spatial size dependence at $m_f a = 0.01-0.04$ observed in the right panel of Fig. 3. Quark masses in this range are heavier than those at $\beta=2.6$ due to a smaller lattice spacing, and hence calculations at smaller values of $m_f a$ are needed to expose finite spatial volume effects at $\beta=2.9$.

VI. B PARAMETERS

A. Extraction of B parameters

In Figs. 7 and 8 we show typical data for the ratio of kaon Green's functions for B_K and B_P defined in Eqs. (3.1) and (3.2) as a function of the temporal site t of the weak operator. The values of these quantities at each m_f , N_σ and N_5 are extracted by fitting the plateau with a constant. The fitting range, determined by the inspection of plots for the ratio and

those for the effective pseudo scalar meson mass, is $12 \leq t \leq 27$ for all simulations at $\beta=2.6$ and $18 \leq t \leq 41$ at $\beta=2.9$. In Tables IV–IX we list the numerical values of B_K and B_P at four quark masses $m_f a = 0.01, 0.02, 0.03, 0.04$ for each set of run parameter.

B. Chiral property for B_P

We have seen in Sec. V that corrections in m_{PS}^2 due to a finite fifth dimensional size N_5 is sufficiently small for $N_5 = 16$ for the range of quark mass m_f explored, and that the non-zero pseudo scalar meson mass at $m_f=0$ is caused by finite spatial size effects. As a further check we investigate the chiral property of the matrix element for the four-quark operator through B_P , which is expected to vanish linearly at $m_f=0$. In Fig. 9 we plot bare values of B_P as a function of $m_f a$ at $\beta=2.6$ and 2.9 . Inspecting the results at $\beta=2.6$ on the left panel of Fig. 9 we observe an agreement for the fifth dimensional size $N_5=16$ (open circle) and 32 (open square). This shows that $N_5=16$ is also large enough for this matrix element.

On the other hand, there is a trend of increase for larger spatial volumes when the quark mass goes below $m_f=0.02$. Finite spatial size effects appear also in this quantity. Making a linear chiral extrapolation, we find a small but negative residual at $m_f=0$. Contrary to the case of m_{PS}^2 , two alternative fits including a quadratic term, $(m_f a)^2$, or a chiral loga-

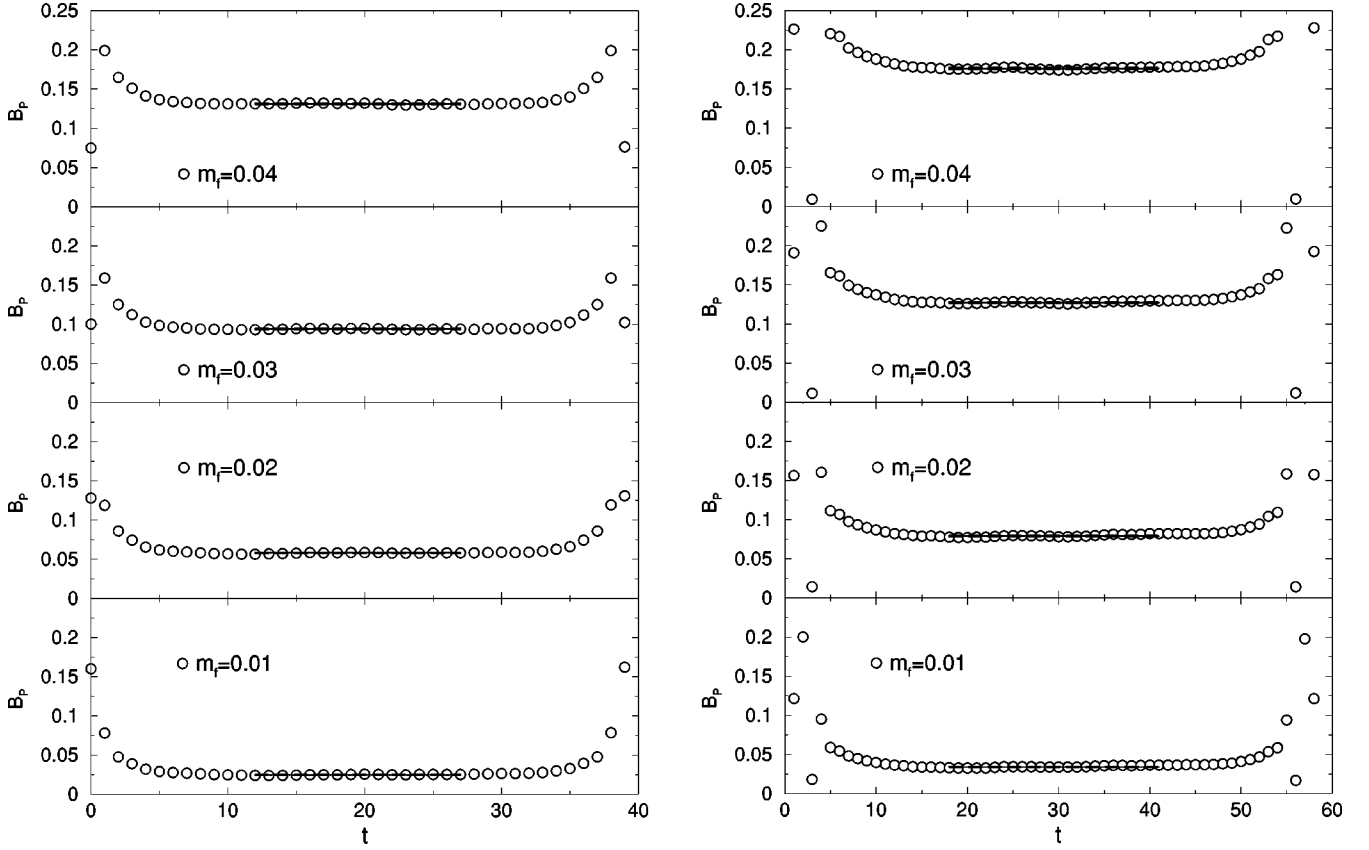


FIG. 8. Ratio of weak matrix element with pseudo scalar density (3.2) as a function of temporal distance t at $\beta=2.6$ on a $24^3 \times 40$ lattice (left) and at $\beta=2.9$ on a $32^3 \times 60 \times 16$ lattice (right). Lines show constant fit over the fitted range.

arithm term, $m_f a \log(m_f a)$, give smaller sizes of the intercept at $m_f=0$ compared to that from the linear fit. We find, however, that sizes of the intercept decrease as N_σ increases for all fits. Therefore we conclude that the non-zero values of B_P at $m_f=0$ are a finite-spatial size effect, and is not a signal of violation of chiral symmetry. Details of the chiral fit are given in the Appendix.

The negative sign of the intercept may be understood as follows. Neglecting the small violation due to the finite N_5 , chiral symmetry implies

$$Z_A \frac{\langle 0|A_\mu|P\rangle}{\langle 0|P|P\rangle} = \frac{2m_f}{m_{PS}}, \quad (6.1)$$

where the bare quantities A_μ and P are local axial vector current and pseudo scalar density, and Z_A is the renormalization factor for A_μ , with which we obtain

$$\begin{aligned} B_P &= \frac{8}{3} B_K \frac{|\langle 0|A_\mu|P\rangle|^2}{|\langle 0|P|P\rangle|^2} = B_K \frac{32m_f^2}{3Z_A^2 m_{PS}^2} \\ &= B_K \frac{32m_f^2}{3Z_A^2 A_{PS}(m_f + m_{\text{res}(fs)})}. \end{aligned} \quad (6.2)$$

This relation is well-satisfied at $\beta=2.6$ where Z_A is non-perturbatively known [20] and is reasonably good with the

perturbative Z_A at $\beta=2.9$. Since $m_{\text{res}(fs)} \ll m_f$ in the range of m_f in our simulation, we approximately obtain

$$B_P \simeq B_K \frac{32}{3Z_A A_{PS}} (m_f - m_{\text{res}(fs)}), \quad (6.3)$$

showing that a positive $m_{\text{res}(fs)}$ implies a negative intercept of B_P . This formula also suggests that the large part of the size effect for B_P is caused by that for m_{PS}^2 .

C. B_K

The bare value of B_K is interpolated as a function of $m_f a$ using a formula suggested by chiral perturbation theory [21],

$$B_K = B[1 - 3c m_f a \log(m_f a) + b m_f a]. \quad (6.4)$$

This interpolation is illustrated in Fig. 10 and its detail is described in the Appendix. The physical value of B_K is obtained at the point $m_f = m_f^s/2$ (solid circles in Fig. 10) which is estimated from the experimental value of m_K/m_ρ . The renormalized values of $B_K(\text{NDR}; \mu=2 \text{ GeV})$ and related physical quantities are collected in Table XI.

We plot the renormalized value of B_K as a function of the spatial size in Fig. 11. Filled circles and triangles are results at $\beta=2.6$ and 2.9 keeping the same fifth dimensional size $N_5=16$. At $\beta=2.6$ we observe a slight increase of B_K from the spatial size $N_\sigma a \approx 1.7 \text{ fm}$ to 2.6 fm , but the values be-

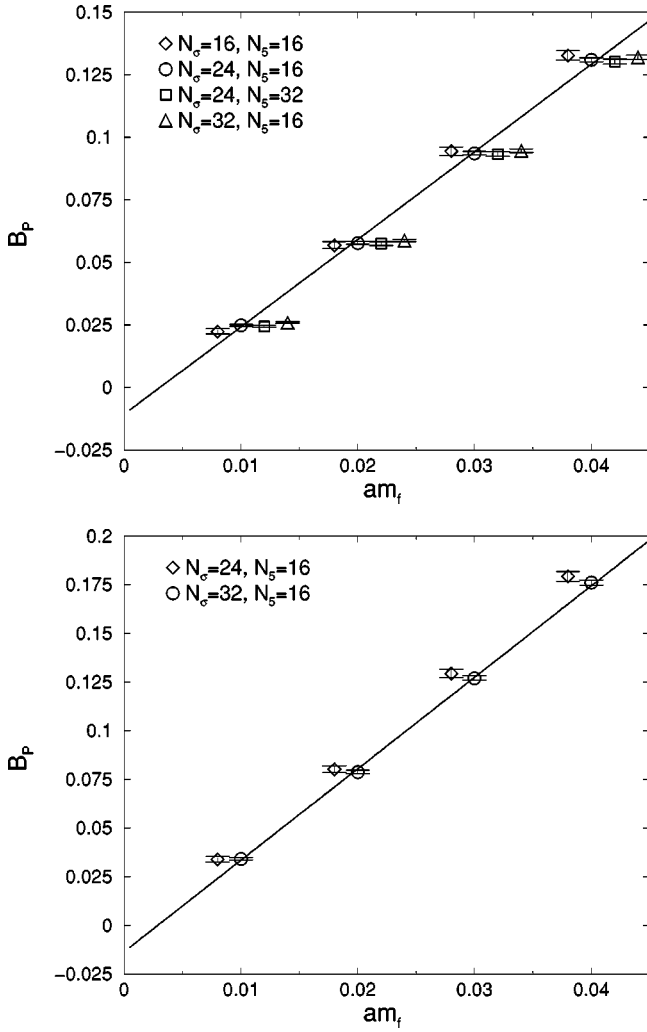


FIG. 9. $B_P(m_f=0)$ vs m_f at $\beta=2.6$ (top) and $\beta=2.9$ (bottom). The data except for the main run are shifted in m_f .

yond the size $N_\sigma a \approx 2.6$ fm are well consistent within the statistical error of 1%. This result agrees with that of a previous finite spatial size study with the Kogut-Susskind quark action [6], which found finite size effects to be smaller than 0.5% for the spatial size $N_\sigma a \geq 2.2$ fm. We conclude that the size of about 2.6 fm ($N_\sigma=24, \beta=2.6$) and 2.3 fm ($N_\sigma=32, \beta=2.9$) used in our main runs is sufficient to avoid spatial size effects for B_K at a 1% level.

In Fig. 12 we plot B_K as a function of the fifth dimensional length N_5 on a $24^3 \times 40$ four-dimensional lattice at $\beta=2.6$. The results at $N_5=32$ and $N_5=16$ are in agreement within the statistical error of 1%. Hence the fifth dimensional size of $N_5=16$ is sufficient for the calculation of B_K at this accuracy.

Our final results from the main runs are shown in Fig. 13 as a function of lattice spacing by filled squares. The open symbols and the associated lines represent results from a previous calculation with the Kogut-Susskind (staggered) quark action [6], where gauge invariant and non-invariant four-quark operators are used. Our result obtained with the domain wall quark action and an RG-improved gluon action show a much better scaling behavior; the central values of

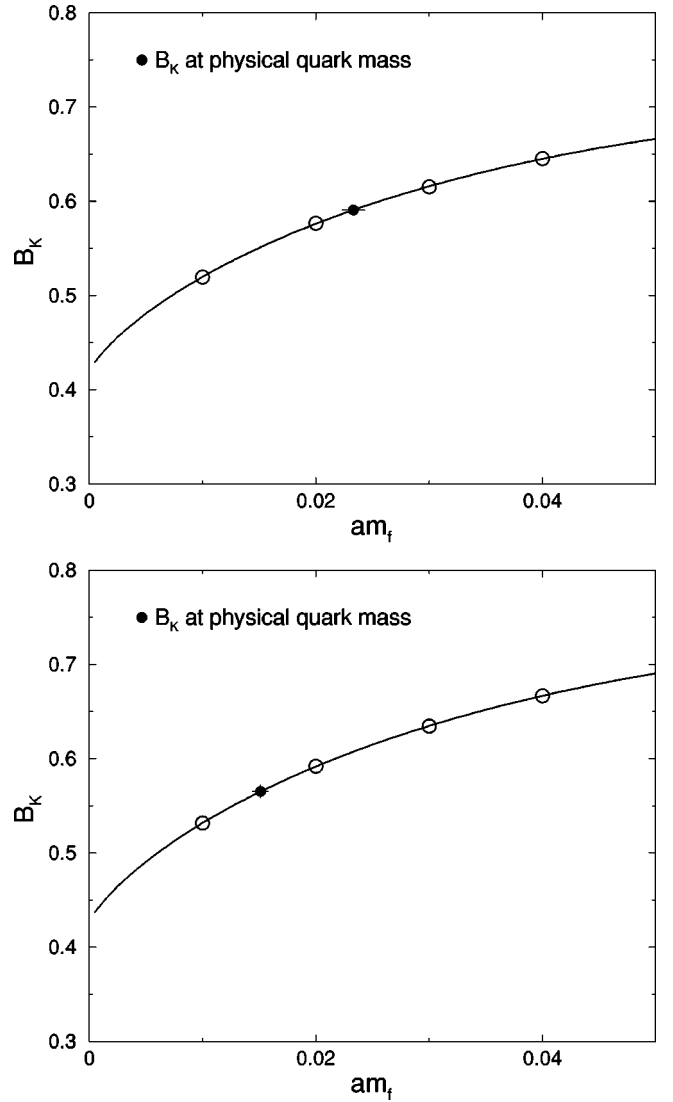


FIG. 10. Bare B_K interpolated as a function of $m_f a$ at $\beta=2.6$ for a $24^3 \times 40 \times 16$ lattice (top) and at $\beta=2.9$ on a $32^3 \times 60 \times 16$ lattice (bottom).

the two points differ by only 1.6% while the Kogut-Susskind results show a 10% decrease over the similar range of lattice spacing $a^{-1} \approx 2-3$ GeV. In order to estimate the continuum value, we then make a constant extrapolation $B_K(a) = B_K$, which yields $B_K(\mu=2 \text{ GeV}) = 0.5746(61)$.

Possible sources of systematic errors in this result are scaling violation ignored in the constant fit and higher loop corrections in the renormalization factors. Making an extrapolation of our data of the form $B_K(a) = B_K + c \cdot a^2$, based on $\mathcal{O}(a^2)$ scaling violation expected for DWQCD [22,23], we obtain an estimate of 2.2% for the first error. A simple estimate for the second error is provided by the value of $\alpha_{\overline{\text{MS}}}(1/a)^2$ at the finer lattice spacing of $\beta=2.9$. This yields 2.5% for the second error. This seems to be a reasonable estimate since other methods of estimation, either shifting the matching scale from $q^* = 1/a$ to $q^* = \pi/a$ or employing different choices of gauge coupling such as Eq. (4.35), give a small variation of $\mathcal{O}(1\%)$. Adding the two estimates by quadrature gives a 3.3% systematic error, and we obtain

TABLE XI. Results for B parameters together with those of relevant quantities, $g = g_P$ in the last row denotes the use of an alternative definition of the coupling (4.35).

β	2.6	2.6	2.6	2.6	2.9	2.9
N_t	40	40	40	40	60	60
N_σ	16	24	24	32	24	32
N_5	16	16	32	16	16	16
a^{-1} (GeV)	1.875(56)	1.807(37)	1.758(51)	1.847(43)	2.869(68)	2.807(55)
Bare B parameters						
B_K	0.575(14)	0.5908(57)	0.5975(77)	0.5871(60)	0.554(14)	0.5655(69)
Renormalized B parameters ($\overline{\text{MS}}$ scheme with NDR at $\mu=2$ GeV)						
$B_K(q^*=1/a)$	0.564(14)	0.5782(55)	0.5839(75)	0.5753(58)	0.558(14)	0.5690(70)
$B_K(q^*=\pi/a)$	0.570(14)	0.5844(56)	0.5901(76)	0.5815(59)	0.563(15)	0.5741(70)
$B_K(g=g_P)$	0.566(14)	0.5803(56)	0.5862(75)	0.5773(59)	0.557(14)	0.5684(70)

$$B_K(\text{NDR}; \mu=2 \text{ GeV}) = 0.5746(61)(191) \quad (6.5)$$

as our estimate of the continuum value of B_K in the $\overline{\text{MS}}$ scheme at $\mu=2$ GeV.

This value lies at the lower edge of the one-standard deviation error band of the result $B_K(\mu=2 \text{ GeV}) = 0.628(42)$ obtained with the Kogut-Susskind action [6]. We recall that the statistical error with the Kogut-Susskind results are at the 0.5–1% level. A significantly larger error of 6.7% in the continuum value arises from the continuum extrapolation incorporating both the a^2 scaling violation and the α_s^2 uncertainty due to the use of one-loop renormalization factor. Making a more detailed check of agreement of results from the two types of quark actions requires a better control of systematic errors, in particular those due to renormalization factors. For this purpose non-perturbative determination of these factors for both cases will be necessary.

The RBC Collaboration carried out a quenched simulation with the domain-wall quark action and a plaquette gluon action at $\beta=6.0$ ($a^{-1} \approx 2$ GeV) on a $16^3 \times 32 \times 16$ lattice.

Employing the method of Ref. [2] to non-perturbatively determine the renormalization factors, they reported a value $B_K(\mu=2 \text{ GeV}) = 0.538(8)$ [28]. This value is 7% smaller than our result. A precise comparison, however, would require examination of spatial size and scaling violation effects in the RBC result and of renormalization factors in our result as discussed above.

D. B_K as a function of m_{PS}^2 in the continuum limit

We have so far discussed the scaling behavior of B_K at the physical quark mass. Our data, in fact, allows us to examine the scaling behavior of B_K over a wide range of quark mass, and derive the mass dependence of B_K in the continuum limit.

In order to compare results at different lattice spacings, we employ m_{PS}^2 in physical units (GeV^2) instead of $m_f a$. In Fig. 14 $B_K(\mu=2 \text{ GeV})$ is given as a function of m_{PS}^2 (GeV^2) at $\beta=2.6, 2.9$ and in the continuum limit. The data are first fitted by

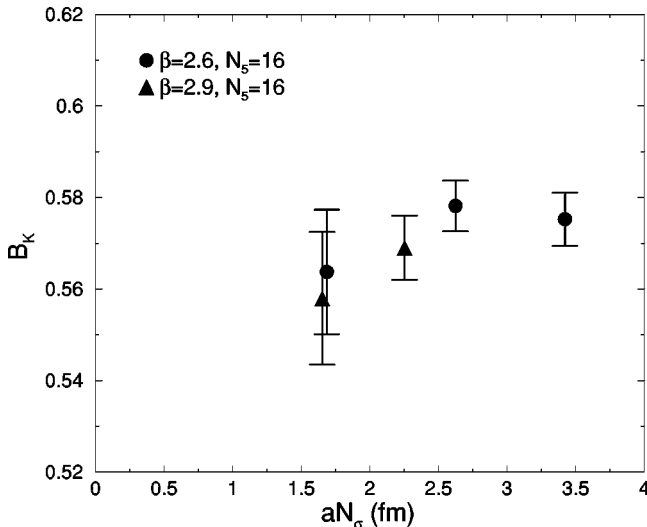


FIG. 11. Renormalized B_K as a function of spatial size.

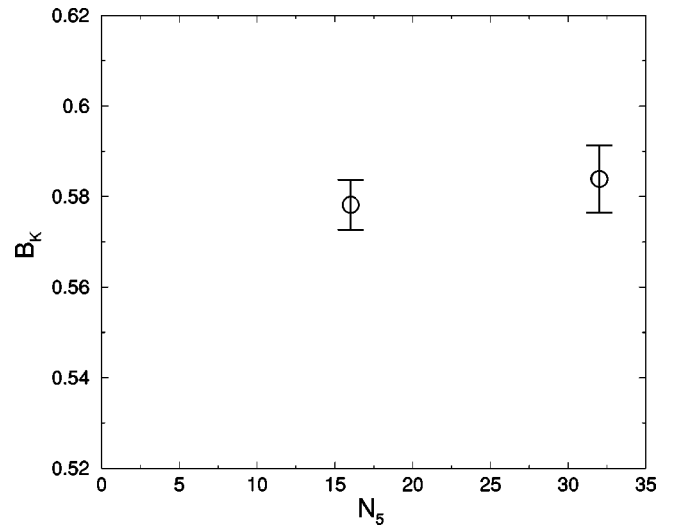


FIG. 12. Renormalized B_K as a function of fifth dimensional length N_5 .

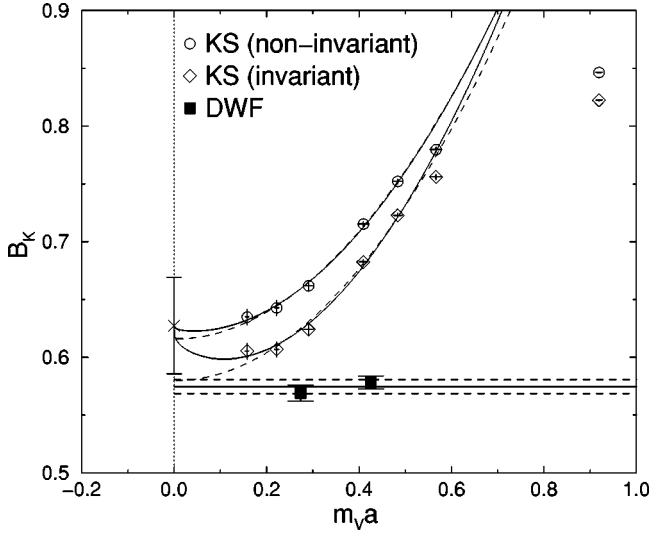


FIG. 13. Scaling behavior of renormalized $B_K(\mu=2 \text{ GeV})$. Previous results with the KS action [6] are also shown with open symbols.

$$B_K = B[1 - 3c_{PS}m_{PS}^2 \log(m_{PS}^2) + b_{PS}m_{PS}^2] \quad (6.6)$$

for each β and then extrapolated to the continuum by a constant fit. All errors in the figure are estimated by a single elimination jackknife procedure, except for fit errors for the continuum extrapolation. As seen in the figure, scaling violation is mild up to $m_{PS}^2 \leq 0.8 \text{ GeV}^2$, and the continuum extrapolation is reliable there. This confirms that the small scaling violation of the physical B_K observed in Sec. VI C is not an accidental one at $m_{PS} = m_K$ but it holds over a wide range of the pseudo scalar meson mass.

In Table XII, values of B_K in the continuum limit, which are also fitted by the same form (6.6), are given for $0.02 \leq m_{PS}^2 \leq 1.0 \text{ (GeV}^2\text{)}$ with errors. Fitted parameters B , b_{PS}

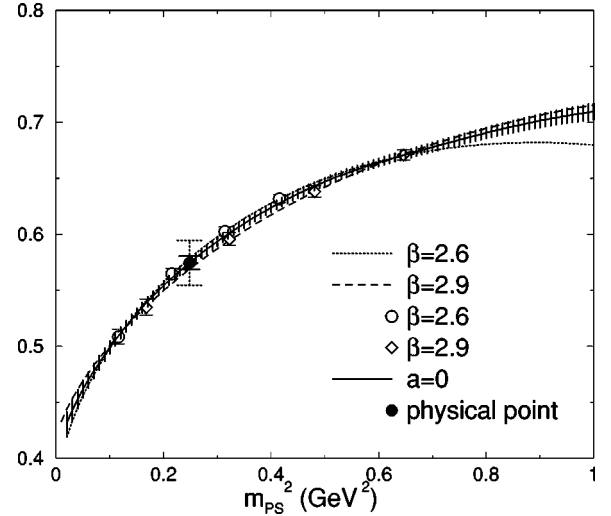


FIG. 14. Renormalized $B_K(\mu=2 \text{ GeV})$ as a function of m_{PS}^2 , at $\beta=2.6, 2.9$ and ∞ (continuum limit), where errors are shown only in the continuum limit. Open symbols represent data obtained in our simulations, while the solid circle gives the value of B_K at the physical point in the continuum limit, with the statistical error (solid) and the total error (dotted).

and c_{PS} are also given in the table, together with the reproduced values. From this result in the continuum limit one can see that the contribution from higher order terms of chiral perturbation theory (b_{PS} and c_{PS}) is non-negligible and becomes as large as 40% of the leading order contribution (B) at $m_{PS} = m_K$. We also comment that our value c_{PS} of the coefficient of the chiral logarithm is 3–4 times smaller than the value predicted by chiral perturbation theory, $1/(4\pi f_\pi)^2 = 0.73 \text{ (GeV}^{-2}\text{)}$. The smallness of this coefficient is also observed in the result of B_K with the KS fermion [6] and may be caused by higher order corrections in chiral perturbation theory, which may not be negligible for values

TABLE XII. Parameters for the fit of B_K in the continuum limit by Eq. (6.6), and B_K as a function of m_{PS}^2 in the continuum limit, together with the reconstruction from the fit.

Parameters	B_K	Error	B_K
B			0.41180
b_{PS}			0.71110
c_{PS}			0.20731
$m_{PS}^2 \text{ (GeV}^2\text{)}$	Continuum extrapolation		Reconstruction by the fit
0.020	0.4318	0.0100	0.4377
0.100	0.4994	0.0058	0.5001
0.200	0.5544	0.0044	0.5528
0.300	0.5937	0.0043	0.5922
0.400	0.6239	0.0041	0.6228
0.500	0.6471	0.0038	0.6470
0.600	0.6643	0.0038	0.6660
0.700	0.6780	0.0043	0.6807
0.800	0.6907	0.0051	0.6918
0.900	0.7016	0.0060	0.6996
1.000	0.7097	0.0075	0.7046

TABLE XIII. Results for quark masses. Renormalized values are in the $\overline{\text{MS}}$ scheme at $\mu=2$ GeV.

β	2.6	2.6	2.6	2.6	2.9	2.9
N_t	40	40	40	40	60	60
N_σ	16	24	24	32	24	32
N_5	16	16	32	16	16	16
a^{-1} (GeV)	1.875(56)	1.807(37)	1.758(51)	1.847(43)	2.869(68)	2.807(55)
Renormalized quark masses ignoring $m_{\text{res}(fs)}$						
$m_{u,d}$ (MeV)	-0.60(90)	0.47(39)	0.82(52)	1.44(37)	3.0(10)	2.12(57)
m_s (MeV)	94.9(33)	96.8(22)	99.8(31)	95.9(24)	94.4(27)	95.4(23)
Renormalized quark masses including $m_{\text{res}(fs)}$						
$m_{u,d}+m_{\text{res}(fs)}$ (MeV)	3.79(12)	3.821(79)	3.92(11)	3.748(92)	3.625(93)	3.701(83)
$m_s+m_{\text{res}(fs)}$ (MeV)	99.3(33)	100.2(21)	102.9(30)	98.3(24)	95.0(24)	97.0(22)
Renormalized s quark mass with ϕ input						
m_s (MeV)	110.(10)	132.(11)	144.(19)	124.8(98)	115.6(58)	120.0(57)

of m_{PS} in our simulation. Possible presence of such higher order corrections, however, does not change our estimate of B_K , obtained by an interpolation of data.

VII. LIGHT QUARK MASSES

We attempt a determination of light quark masses $m_{ud} \equiv (m_u + m_d)/2$ and m_s using our meson mass data. There is a difficulty associated with a non-zero pseudo scalar meson mass at $m_f=0$ due to finite spatial sizes, which is represented by $m_{\text{res}(fs)}$ in the linear chiral formula (5.1). This causes systematic uncertainties in the results for quark masses, which is quite sizable for light u and d quarks.

In order to examine this problem, we calculate the physical quark masses in two ways which differ in the choice of origin for bare quark mass. In the first method we take $m_f=0$ as the origin, and write

$$m_{ud} = Z_q m_f^{ud}, \quad (7.1)$$

$$m_s = Z_q (m_f^s - m_f^{ud}). \quad (7.2)$$

Here m_f^{ud} and m_f^s are the bare quark mass m_f for the physical point of pion and kaon determined by Eqs. (5.3) and (5.4). The subtraction of m_f^{ud} in the second equation is to take into account the contribution of u - d quark in the kaon mass, $m_K \propto m_{ud} + m_s$, and Z_q denotes the renormalization factor to match the bare lattice value to that in the continuum in the $\overline{\text{MS}}$ scheme with NDR at $\mu=2$ GeV as discussed in Sec. IV.

In the second case we take the point $m_f = -m_{\text{res}(fs)}$, where pseudo scalar meson mass vanishes, as the origin. The formula then reads

$$m_{ud} = Z_q (m_f^{ud} + m_{\text{res}(fs)}), \quad (7.3)$$

$$m_s = Z_q (m_f^s - m_f^{ud} + m_{\text{res}(fs)}). \quad (7.4)$$

On the other hand the strange quark mass with the phi meson mass as input is given directly as

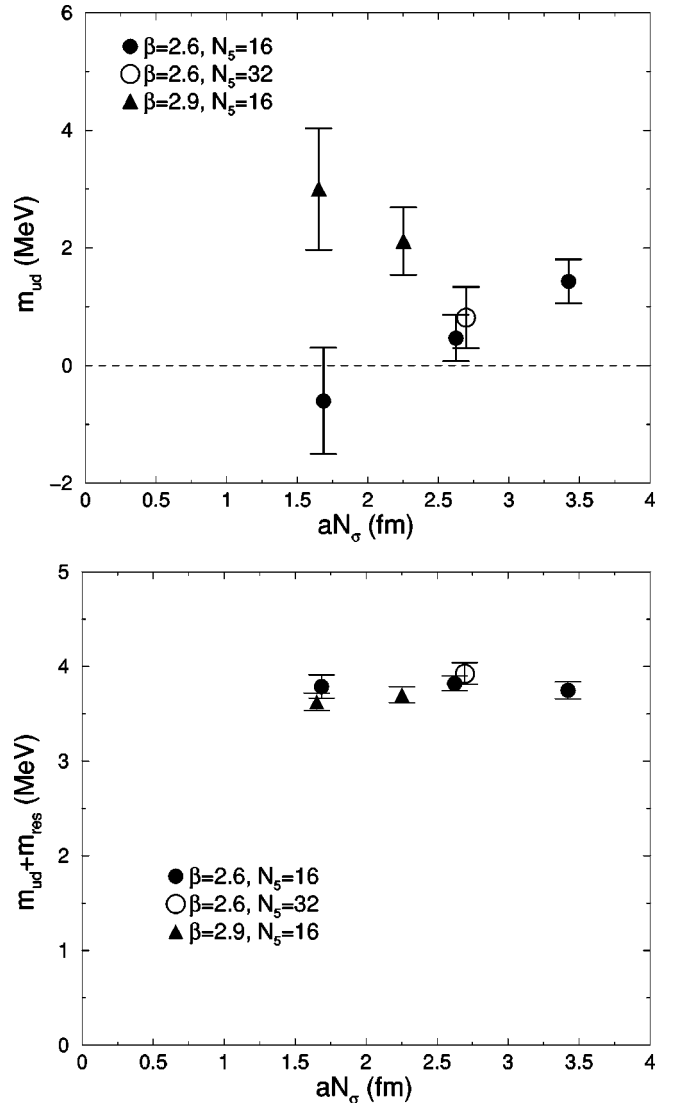


FIG. 15. Renormalized u - d quark mass as a function of spatial size. Results with (top) and without $m_{\text{res}(fs)}$ added (bottom) are shown.

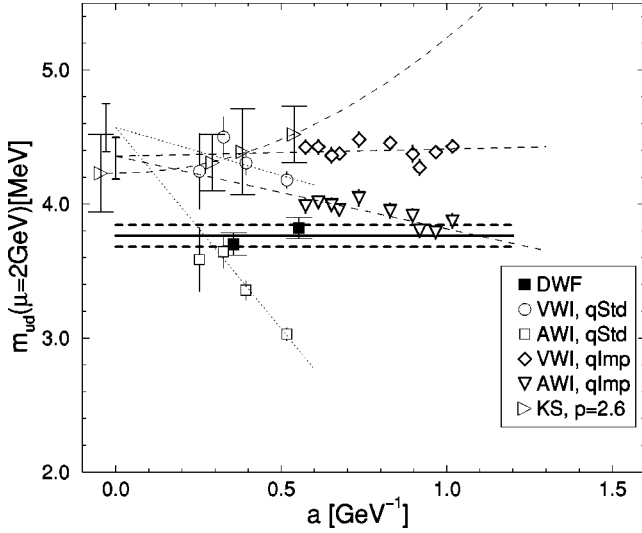


FIG. 16. Scaling behavior of u - d quark mass, calculated with $m_{\text{res}(f_s)}$ added, compared with those from 4-dimensional quark action: Wilson action (Std) [24], clover-improved action (Imp) [25], and Kogut-Susskind (KS) [26] actions. VWI and AWI represent vector and axial-vector Ward-Takahashi identity masses, respectively, p for the KS fermion represents the matching scale of the RI scheme in units of GeV.

$$m_s = Z_q m_s(\phi). \quad (7.5)$$

The results of these calculations are listed in Table XIII.

In Fig. 15 we plot the u - d quark mass calculated in the two ways above as a function of spatial size aN_σ in physical units. Two features are quite evident from this figure. (i) There is little dependence on the fifth dimensional size N_5 .

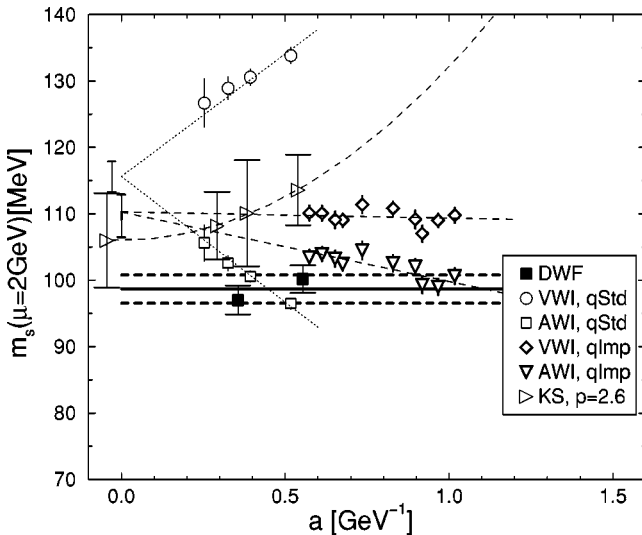


FIG. 17. Scaling behavior of the strange quark mass with K input, calculated with $m_{\text{res}(f_s)}$ added, compared with those from 4-dimensional quark action: Wilson action (Std) [24], clover-improved action (Imp) [25], and Kogut-Susskind (KS) [26] actions. VWI and AWI represent vector and axial-vector Ward-Takahashi identity masses, respectively, p for the KS fermion represents the matching scale of the RI scheme in units of GeV.

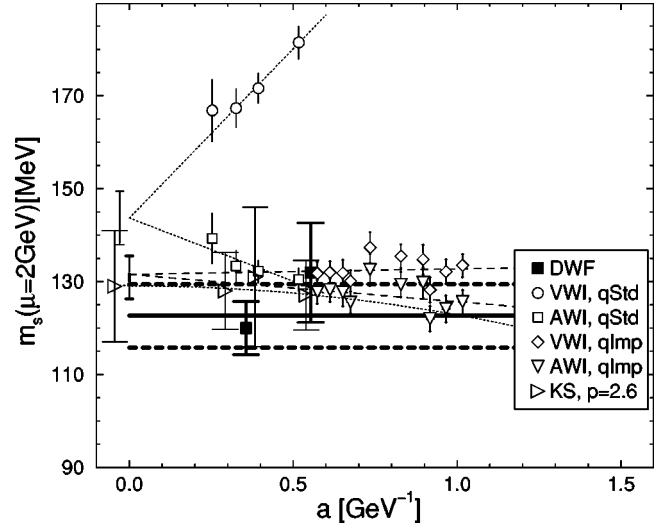


FIG. 18. Scaling behavior of the strange quark mass with ϕ input, compared with those from 4-dimensional quark action: Wilson action (Std) [24], clover-improved action (Imp) [25], and Kogut-Susskind (KS) [26] actions. VWI and AWI represent vector and axial-vector Ward-Takahashi identity masses, respectively, p for the KS fermion represents the matching scale of the RI scheme in units of GeV.

Hence $N_5 = 16$ is sufficient to avoid effects of chiral symmetry breaking at our range of lattice spacings. (ii) Effects of finite spatial size, by contrast, are quite significant if $m_{\text{res}(f_s)}$ is ignored, even yielding a negative value for m_{ud} for small spatial sizes (left panel of Fig. 15). The values calculated including $m_{\text{res}(f_s)}$, on the other hand, are much more stable as a function of aN_σ (right panel).

In order to understand the second point, we note that $m_{\text{res}(f_s)}a$ depends strongly on the volume while the slope A_{PS} is almost volume independent. Using Eq. (5.3) and the corresponding one at $N_\sigma = \infty$ given by

$$\frac{\sqrt{A_{PS}(N_\sigma = \infty) \cdot m_f^{ud}(N_\sigma = \infty)} a}{A_V + B_V m_f^{ud} a} = \frac{m_\pi}{m_\rho}, \quad (7.6)$$

and neglecting a small volume dependence of the denominator $A_V + B_V m_f^{ud} a$, we observe that the following formula holds:

$$\frac{m_f^{ud} - m_f^{ud}(N_\sigma = \infty)}{m_f^{ud}(N_\sigma = \infty)} = - \frac{m_{\text{res}(f_s)}}{m_f^{ud}(N_\sigma = \infty)} - \frac{A_{PS} - A_{PS}(N_\sigma = \infty)}{A_{PS}}. \quad (7.7)$$

Since the magnitude $m_{\text{res}(f_s)} \approx 2-3$ MeV for our spatial size of $aN_\sigma \approx 2.5$ fm is comparable to the actual u - d quark mass, the first term is $\mathcal{O}(1)$ and becomes the main contribution to the size effect, while the second term, representing finite size effect in the slope A_{PS} , is found to be much smaller. Hence including $m_{\text{res}(f_s)}$ removes a dominant part of finite size ef-

TABLE XIV. Results for light quark masses as compared with previous studies. One-loop approximation to the renormalization factors are employed except for those with the KS fermion action in the last row.

Ref.	Quark action	Gluon action	$\overline{m}_{ud}^{\text{MS}}(2\text{GeV})$	$\overline{m}_s^{\text{MS}}(2\text{GeV})$	
				K input	ϕ input
This work	DW	RG-improved	3.764(81)(215) MeV	98.7(2.1)(5.6) MeV	122.6(6.8)(13) MeV
[24]	Wilson	plaquette	4.57(18) MeV	116 (3) MeV	144 (6) MeV
[25]	clover	RG-improved	$4.36_{-0.17}^{+0.14}$ MeV	110_{-4}^{+3} MeV	132_{-6}^{+4} MeV
[26]	KS	plaquette	4.23(29) MeV	106 (7) MeV	129 (12) MeV

fects in u - d quark mass. In view of this situation we take the values including $m_{\text{res}(\text{fs})}$ as the best estimate from our present data for m_{ud} .

The scaling behavior of m_{ud} is plotted in Fig. 16 by filled squares. Making a constant fit to the two values, we find

$$\overline{m}_{ud}^{\text{MS}}(2 \text{ MeV}) = 3.764(81)(215) \text{ MeV}, \quad (7.8)$$

where the first error is statistical and the second due to scaling violation and $\mathcal{O}(\alpha^2)$ systematic errors estimated in the same way as for B_K (see Sec. VI C) and added in quadrature.

For the heavier s quark, effects of $m_{\text{res}(\text{fs})}$ are less significant, and those of N_5 are within the statistical error, as one can see in Table XIII. In parallel with u - d quark mass we take the results including $m_{\text{res}(\text{fs})}$ as our best estimate. The two values from our main runs at $\beta=2.6$ and 2.9 are plotted by filled squares in Figs. 17 (K input) and 18 (ϕ input). Fitting with a constant and making estimation of systematic errors as for m_{ud} we obtain

$$\overline{m}_s^{\text{MS}}(2\text{MeV}) = \begin{cases} 98.7(2.1)(5.6) \text{ MeV} & K \text{ input} \\ 122.6(6.8)(13) \text{ MeV} & \phi \text{ input.} \end{cases} \quad (7.9)$$

In Figs. 16, 17 and 18 open symbols show results obtained with the conventional 4-dimensional quark actions; circles and squares for the Wilson action with the plaquette gluon action [24], diamonds and down triangles for the clover action with the RG-improved gluon action as used in the present work [25], and right triangles for the Kogut-Susskind quark action with the plaquette gluon action [26]. The first two cases use one-loop renormalization factors, while the Kogut-Susskind results are based on a non-perturbative value calculated in the RI scheme. The values estimated in the continuum limit in each of these studies are plotted at $a=0$ and are summarized in Table XIV.

Compared to the values obtained with the 4-dimensional quark actions, our results with the domain-wall action are somewhat small both for u - d and s quark. As with the case

TABLE XV. Chiral extrapolation of $m_{p_S}^2 a^2$ by different fits.

β	2.6	2.6	2.6	2.6	2.9	2.9
N_t	40	40	40	40	60	60
N_σ	16	24	24	32	24	32
N_5	16	16	32	16	16	16
Linear fit $m_{p_S}^2 a^2 = A_{p_S}(m_{\text{res}(\text{fs})} a + m_f a)$						
$m_{\text{res}(\text{fs})} a$	0.00201(42)	0.00161(18)	0.00153(23)	0.00108(17)	0.00019(31)	0.00049(17)
A_{p_S}	2.983(36)	3.050(16)	3.040(19)	3.053(22)	2.017(19)	2.012(15)
$\chi^2/\text{d.o.f}$	0.26(13)	0.073(55)	0.069(60)	0.114(82)	0.71(22)	0.88(26)
Quadratic fit $m_{p_S}^2 a^2 = A_{p_S}(m_{\text{res}(\text{fs})} a + m_f a) + B_{p_S}(m_f a)^2$						
$m_{\text{res}(\text{fs})} a$	0.00293(49)	0.00177(18)	0.00174(25)	0.00131(21)	0.00125(37)	0.00129(22)
A_{p_S}	2.765(76)	3.005(39)	2.986(48)	2.987(50)	1.817(44)	1.856(36)
B_{p_S}	4.5(1.1)	0.95(60)	1.12(72)	1.39(66)	4.13(63)	3.31(50)
$\chi^2/\text{d.o.f}$	0.0012(30)	0.046(19)	0.034(17)	0.041(16)	0.0003(17)	0.024(12)
Chiral logarithm $m_{p_S}^2 a^2 = A_{p_S}(m_{\text{res}(\text{fs})} a + m_f a) + C_{p_S} m_f a \log(m_f a)$						
$m_{\text{res}(\text{fs})} a$	0.00284(37)	0.00180(18)	0.00178(25)	0.00138(22)	0.00162(29)	0.00157(19)
A_{p_S}	3.55(13)	3.163(72)	3.175(85)	3.221(69)	2.538(73)	2.428(55)
C_{p_S}	0.202(51)	0.041(28)	0.048(33)	0.060(30)	0.187(29)	0.148(23)
$\chi^2/\text{d.o.f}$	0.0102(66)	0.059(17)	0.045(15)	0.058(15)	0.0159(96)	0.073(17)

TABLE XVI. Chiral extrapolation of m_V by linear fit.

β	2.6	2.6	2.6	2.6	2.9	2.9
N_t	40	40	40	40	60	60
N_σ	16	24	24	32	24	32
N_5	16	16	32	16	16	16
Linear fit $m_V a = A_V + B_V m_f a$						
A_V	0.411(12)	0.4256(85)	0.437(12)	0.4153(97)	0.2661(63)	0.2727(53)
B_V	2.63(24)	2.19(18)	2.01(26)	2.34(19)	2.55(13)	2.43(11)
$\chi^2/\text{d.o.f}$	0.002(18)	0.30(25)	0.22(23)	0.14(15)	0.0015(89)	0.06(14)

of B_K , a more precise examination of the issue of agreement of the continuum value requires a non-perturbative determination of the renormalization factors for our combination of quark and gluon actions.

We note that a recent result $m_s = 110(2)(22)$ MeV [27] with K input using domain wall fermions and non-perturbative renormalization factor but with the plaquette gauge action at $\beta=6.0$ is consistent with ours, within the 20% systematic error quoted which includes that associated with the conversion from the RI scheme to the $\overline{\text{MS}}$ scheme.

VIII. CONCLUSIONS

In this article we have presented our investigation of quenched calculation of the kaon B parameter B_K with domain-wall QCD.

In order to make full use of the good chiral property of this system, we employed a renormalization-group improved gluon action and carried out simulations at $a^{-1} \geq 2$ GeV. According to our previous study [14], the magnitude of chiral symmetry breaking due to finite fifth dimensional size N_5 ,

if measured in terms of residual quark mass m_{5q} , is less than 1 MeV for $N_5 \geq 10$ at such lattice spacings. An explicit examination of the N_5 dependence of B_K has shown that such effect is less than 1% for $N_5 \geq 16$ at $a^{-1} \geq 2$ GeV.

We have also found that spatial size effects are less than 1% for the physical spatial sizes $aN_\sigma \geq 2.5$ fm, confirming the finding of a previous study with the Kogut-Susskind quark action. Furthermore, scaling violation turned out to be very small, being less than 2% between $a^{-1} \approx 2$ GeV and 3 GeV.

These results show that DWQCD, albeit computer time consuming by a factor $\mathcal{O}(N_5)$ compared to conventional lattice QCD simulations, provides a very good framework for a precision determination of B_K . An important ingredient toward this goal, which was not available for the present study, is the value of the renormalization factors precise to the level of one percent. Results using the RI scheme have been reported for the plaquette action by the RBC Collaboration [28], and an attempt employing the Schrödinger functional technique is in progress [20]. Hopefully progress in these calculations will allow us to report results for B_K in the con-

TABLE XVII. Chiral extrapolation of B_P by different fits.

β	2.6	2.6	2.6	2.6	2.9	2.9
N_t	40	40	40	40	60	60
N_σ	16	24	24	32	24	32
N_5	16	16	32	16	16	16
Linear fit $B_P = A_{B_P} + B_{B_P} m_f a$						
A_{B_P}	-0.0146(13)	-0.01064(48)	-0.01094(54)	-0.00933(45)	-0.0149(16)	-0.01340(69)
B_{B_P}	3.652(62)	3.497(26)	3.492(31)	3.481(29)	4.823(71)	4.699(39)
$\chi^2/\text{d.o.f}$	0.99(45)	7.2(1.1)	3.57(63)	8.6(1.0)	0.58(26)	2.65(62)
Quadratic fit $B_P = A_{B_P} + B_{B_P} m_f a + C_{B_P} (m_f a)^2$						
A_{B_P}	-0.0104(14)	-0.00599(54)	-0.00682(59)	-0.00461(49)	-0.0107(18)	-0.00869(75)
B_{B_P}	3.18(14)	2.969(55)	3.022(63)	2.931(51)	4.36(15)	4.160(86)
C_{B_P}	10.1(2.3)	11.45(90)	10.17(90)	12.18(74)	9.8(2.3)	11.6(1.4)
$\chi^2/\text{d.o.f}$	0.129(69)	0.335(88)	0.187(57)	0.324(89)	0.086(43)	0.299(73)
Chiral logarithm $B_P = A_{B_P} + B_{B_P} m_f a + D_{B_P} m_f a \log(m_f a)$						
A_{B_P}	-0.0058(20)	-0.00093(81)	-0.00232(83)	0.00067(69)	-0.0062(24)	-0.0035(12)
B_{B_P}	4.96(29)	4.97(11)	4.80(10)	5.042(89)	6.10(28)	6.21(17)
D_{B_P}	0.46(11)	0.519(41)	0.461(41)	0.546(33)	0.45(10)	0.532(63)
$\chi^2/\text{d.o.f}$	0.056(40)	0.059(30)	0.040(23)	0.046(30)	0.039(24)	0.121(39)

TABLE XVIII. Chiral extrapolation of B_K with chiral logarithm.

β	2.6	2.6	2.6	2.6	2.9	2.9
N_t	40	40	40	40	60	60
N_σ	16	24	24	32	24	32
N_5	16	16	32	16	16	16
Chiral logarithm $B_K = B(1 - 3cm_f a \log(m_f a) + bm_f a)$						
B	0.340(43)	0.420(16)	0.425(19)	0.443(11)	0.369(42)	0.427(16)
b	-26(12)	-10.7(3.0)	-10.6(3.1)	-6.1(2.2)	-21.9(9.9)	-10.3(3.5)
c	5.0(1.8)	2.50(46)	2.42(49)	1.80(32)	4.4(1.6)	2.52(50)
$\chi^2/\text{d.o.f}$	0.009(22)	0.043(43)	0.020(24)	0.075(52)	0.025(39)	0.009(21)

tinuum limit with a total error of at most a few percent in quenched QCD in the near future.

We have also examined the possibility of calculating light quark masses in DWQCD. We find good scaling behavior, and the values estimated for the continuum limit are in reasonable agreement, albeit somewhat small, with those of 4-dimensional simulations. Further progress toward precision determination of light quark masses also requires that of renormalization factors at the few percent level.

ACKNOWLEDGMENTS

This work is supported in part by Grants-in-Aid of the Ministry of Education (Nos. 10640246, 10640248, 10740107, 11640250, 11640294, 11740162, 12014202, 12304011, 12640253, 12740133, 13640260). S.E., T.K., K.N., J.N., and H.P.S. are supported by J.S.P.S. A.A.K. is supported by JSPS Research for the Future Program (No. JSPS-RFTF 97P01102).

APPENDIX: CHIRAL FIT

The chiral extrapolation of our data is made by uncorrelated fit and errors of parameters are estimated by a single elimination jackknife procedure.

For pseudo scalar meson mass we investigate the following three types of fits:

$$m_{PS}^2 a^2 = A_{PS}(m_{\text{res(fs)}} a + m_f a), \quad (\text{A1})$$

$$m_{PS}^2 a^2 = A_{PS}(m_{\text{res(fs)}} a + m_f a) + B_{PS}(m_f a)^2, \quad (\text{A2})$$

$$m_{PS}^2 a^2 = A_{PS}(m_{\text{res(fs)}} a + m_f a) + C_{PS} m_f a \log(m_f a). \quad (\text{A3})$$

The results of the fits are given in Table XV together with $\chi^2/\text{d.o.f}$. It is found that the three types of fits in the above yield almost identical values of the pseudo scalar meson mass at $m_f=0$. The result of the chiral fit for vector meson mass

$$m_V a = A_V + B_V m_f a \quad (\text{A4})$$

is given in Table XVI.

The bare value of B_P is fitted with three types of functional form given by

$$B_P = A_{B_P} + B_{B_P} m_f a, \quad (\text{A5})$$

$$B_P = A_{B_P} + B_{B_P} m_f a + C_{B_P} (m_f a)^2, \quad (\text{A6})$$

$$B_P = A_{B_P} + B_{B_P} m_f a + D_{B_P} m_f a \log(m_f a). \quad (\text{A7})$$

The last two fits with nonlinear terms lead to a smaller magnitude of the chiral symmetry breaking term A_{B_P} as is seen in Table XVII where values of the coefficients are also given.

The bare value of B_K is fitted with chiral logarithm

$$B_K = B[1 - 3cm_f a \log(m_f a) + bm_f a] \quad (\text{A8})$$

and the results are given in Table XVIII.

- [1] For recent reviews, see, Y. Kuramashi, Nucl. Phys. B (Proc. Suppl.) **83**, 24 (2000); L. Lellouch, hep-lat/0011088.
[2] G. Martinelli, C. Pittori, C. T. Sachrajda, M. Testa, and A. Vladikas, Nucl. Phys. **B445**, 81 (1995); A. Donini *et al.*, Phys. Lett. B **360**, 83 (1995); M. Crisafulli *et al.*, *ibid.* **369**, 325 (1996); L. Conti *et al.*, *ibid.* **421**, 273 (1998); C. R. Allton

et al., *ibid.* **453**, 30 (1999); A. Donini, V. Gimenez, L. Giusti, and G. Martinelli, *ibid.* **470**, 233 (1999).

- [3] R. Gupta, T. Bhattacharya, and S. Sharpe, Phys. Rev. D **55**, 4036 (1997).
[4] JLQCD Collaboration, S. Aoki *et al.*, Phys. Rev. Lett. **81**, 1778 (1998); Phys. Rev. D **60**, 034511 (1999).

- [5] G. Kilcup *et al.*, Phys. Rev. Lett. **64**, 25 (1990); S. Sharpe *et al.*, Nucl. Phys. B (Proc. Suppl.) **26**, 197 (1992).
- [6] JLQCD Collaboration, S. Aoki *et al.*, Phys. Rev. Lett. **80**, 5271 (1998).
- [7] D. Kaplan, Phys. Lett. B **288**, 342 (1992).
- [8] Y. Shamir, Nucl. Phys. **B406**, 90 (1993).
- [9] V. Furman and Y. Shamir, Nucl. Phys. **B439**, 54 (1995).
- [10] R. Narayanan and H. Neuberger, Nucl. Phys. **B443**, 305 (1995).
- [11] H. Neuberger, Phys. Lett. B **417**, 141 (1998); **427**, 353 (1998); Phys. Rev. D **57**, 5417 (1998).
- [12] T. Blum and A. Soni, Phys. Rev. D **56**, 174 (1997); Phys. Rev. Lett. **79**, 3595 (1997); hep-lat/9712004.
- [13] Y. Iwasaki, Report No. UTHEP-118, 1983; Nucl. Phys. **B258**, 141 (1985).
- [14] CP-PACS Collaboration, A. Ali Khan *et al.*, Phys. Rev. D **63**, 114504 (2001); Nucl. Phys. B (Proc. Suppl.) **83-84**, 591 (2000).
- [15] T. Blum, P. Chen, N. Christ, C. Cristian, C. Dawson, G. Fleming, A. Kaehler, X. Liao, G. Liu, C. Malureanu, R. Mawhinney, S. Ohta, G. Siegert, A. Soni, C. Sui, P. Vranas, M. Wingate, L. Wu, and Y. Zhestkov, hep-lat/0007038; P. Chen, N. Christ, G. Fleming, A. Kaehler, C. Malureanu, R. Mawhinney, G. Siegert, C. Sui, P. M. Vranas, and Y. Zhestkov, hep-lat/9812011; L. Wu *et al.*, Nucl. Phys. B (Proc. Suppl.) **83-84**, 224 (2000); G. T. Fleming *et al.*, *ibid.* **83-94**, 363 (2000).
- [16] S. Aoki, T. Izubuchi, Y. Kuramashi, and Y. Taniguchi, Phys. Rev. D **59**, 094505 (1999); **60**, 114504 (1999); (in preparation).
- [17] A. J. Buras, M. Jamin, and P. H. Weisz, Nucl. Phys. **B347**, 491 (1990).
- [18] K. G. Chetyrkin, Phys. Lett. B **404**, 161 (1997).
- [19] S. Aoki, T. Umemura, M. Fukugita, N. Ishizuka, H. Mino, M. Okawa, and A. Ukawa, Phys. Rev. D **50**, 486 (1994).
- [20] CP-PACS Collaboration, in progress.
- [21] S. Sharpe, Phys. Rev. D **46**, 3146 (1992).
- [22] T. Blum, A. Soni, and M. Wingate, Phys. Rev. D **60**, 114507 (1999).
- [23] J. Naoki and Y. Taniguchi, Phys. Rev. D **61**, 054505 (2000).
- [24] CP-PACS Collaboration, S. Aoki *et al.*, Phys. Rev. Lett. **84**, 238 (2000).
- [25] CP-PACS Collaboration, A. Ali Khan *et al.*, hep-lat/0004010.
- [26] JLQCD Collaboration, S. Aoki *et al.*, Phys. Rev. Lett. **82**, 4392 (1999).
- [27] M. Wingate, hep-lat/0009022; Nucl. Phys. B (Proc. Suppl.) **94**, 277 (2001).
- [28] RBC Collaboration, T. Blum, Nucl. Phys. B (Proc. Suppl.) **94**, 291 (2001); C. Dawson, *ibid.* **94**, 613 (2001).